IMMUNOLOGY

Phosphorylation of serine-893 in CARD11 suppresses the formation and activity of the CARD11-BCL10-MALT1 complex in T and B cells

Kerstin Kutzner[1]†, Simone Woods[1]†, Ozge Karayel[2], Torben Gehring[1], Hongli Yin[1], Andrew Flatley[3], Carina Graß[1], Nicole Wimberger[1], Marie J. Tofaute[1], Thomas Seeholzer[1], Regina Feederle[3], Matthias Mann[2], Daniel Krappmann[1]*

AQ1

CARD11 acts as a gatekeeper for adaptive immune responses after T cell or B cell antigen receptor (TCR/BCR) ligation on lymphocytes. PKCθ/β-catalyzed phosphorylation of CARD11 promotes the assembly of the CARD11-BCL10-MALT1 (CBM) complex and lymphocyte activation. Here, we demonstrated that PKCθ-dependent CARD11 phosphorylation also suppressed CARD11 functions in T or B cells. Through mass spectrometry–based proteomics analysis, we identified multiple constitutive and inducible CARD11 phosphorylation sites in T cells. We demonstrated that a single TCR- or BCR-inducible phosphorylation on Ser^{893} in the carboxyl terminus of CARD11 prevented the activation of the transcription factor NF-κB, the kinase JNK, and the protease MALT1. Moreover, CARD11 Ser^{893} phosphorylation sensitized BCR-addicted lymphoma cells to toxicity induced by Bruton's tyrosine kinase (BTK) inhibitors. Phosphorylation of Ser^{893} in CARD11 by PKCθ controlled the strength of CARD11 scaffolding by impairing the formation of the CBM complex. Thus, PKCθ simultaneously catalyzes both stimulatory and inhibitory CARD11 phosphorylation events, which shape the strength of CARD11 signaling in lymphocytes.

INTRODUCTION

Antigen binding to the cognate T and B cell receptors (TCR/BCR) on lymphocytes is critical for the initiation of an adaptive immune response. Antigen-induced assembly of caspase recruitment domain family member 11 (CARD11; also termed CARMA1), B cell lymphoma/leukemia protein 10 (BCL10), and mucosa-associated lymphoid tissue protein 1 (MALT1) into the CARD11-BCL10-MALT1 (CBM) signaling complex is a key step in the activation of canonical IKK (IκB kinase)/NF-κB (nuclear factor κB) and JNK (c-Jun N-terminal kinase) signaling (*1*, *2*). CBM complex formation also triggers the activation of the protease MALT1, which modulates immune responses in T and B cells by cleaving substrates involved in cell signaling, gene transcription, and mRNA metabolism (*3*). The CBM complex not only induces a productive immune response in activated effector T cells but also controls peripheral tolerance by promoting the development and function of regulatory T (T_{reg}) cells (*4*–*7*). Although defective CBM complex signaling causes combined immune deficiency, chronic CBM complex activity drives survival and proliferation of aggressive lymphomas addicted to oncogenic activation of the BCR signaling pathway (*8*, *9*). Thus, regulation of CBM complex assembly orchestrates the balance between immune activation and tolerance, and deregulation of these processes induces severe immune pathologies and cancer.

In the CBM complex, CARD11 acts as a molecular seed that recruits preassembled BCL10-MALT1 dimers, thereby inducing BCL10 oligomerization and formation of BCL10-MALT1 filaments (*10*–*13*). In resting lymphocytes, the multidomain scaffold CARD11 is maintained in a closed, autoinhibited state (*14*). The central linker region of CARD11 acts as an inhibitory domain (ID) containing several repressive elements (REs), which make multiple intramolecular contacts with the N-terminal CARD (caspase recruitment domain), the CC (coiled-coil) domain, and the C-terminal MAGUK (membrane-associated guanylate kinase) region (*15*, *16*). Upon lymphocyte activation, these intramolecular associations are released and CARD11 converts to an open and signaling-active conformation (*17*). The conformational rearrangements that control CARD11 scaffolding are regulated by posttranslational modifications (*18*). Upon antigenic stimulation, phosphorylation of Ser^{559} and Ser^{652} in CARD11 by protein kinase Cθ (PKCθ) in T cells and PKCβ in B cells induces the open, active conformation, which allows BCL10 recruitment (*19*–*21*). In addition, by phosphorylating Ser^{562}, IKKβ triggers a positive feedback loop to activate robust CBM complex formation (*22*–*24*). Further, phosphorylation events mediated by AKT, hematopoietic progenitor kinase 1 (HPK1), and calcium/calmodulin-dependent protein kinase II (CamKII) in the ID or the CARD-CC regions facilitate CARD11-dependent downstream signaling (*20*, *25*, *26*). Moreover, CARD11 binding and catalytic activity of casein kinase1α (CK1α) trigger CBM complex formation, but CK1α-catalyzed CARD11 Ser^{615} phosphorylation also counteracts NF-κB activation (*27*, *28*). Thus, CARD11 is controlled by stimulatory and inhibitory phosphorylation events, but how the interplay between these phosphorylation events coordinates its scaffolding function remains unknown (*29*).

Global phosphoproteomic approaches in T or B cells have defined various putative CARD11 phosphorylation sites, but functional characterization of these sites has not been performed (*30*, *31*). By mapping the phosphosites on CARD11 by immunoprecipitation–mass spectrometry (IP-MS), we identified inducible C-terminal Ser^{893} CARD11 phosphorylation as a critical inhibitory modification for

[1]Research Unit Cellular Signal Integration, Helmholtz Zentrum München–German Research Center for Environmental Health. Ingolstaedter Landstr. 1, 85764 Neuherberg, Germany. [2]Department of Proteomics and Signal Transduction, Max Planck Institute of Biochemistry, Am Klopferspitz 18, 82152 Planegg, Germany. [3]Monoclonal Antibody Core Facility, Institute for Diabetes and Obesity, Helmholtz Zentrum München–German Research Center for Environmental Health, Ingolstaedter Landstr. 1, 85764 Neuherberg, Germany.
*Corresponding author: Email: daniel.krappmann@helmholtz-muenchen.de
†These authors contributed equally to this work.

the coordination of complex assembly, activation, and signaling downstream of the CBM in T and B cells.

AQ2 ## RESULTS

MS-based proteomics analysis identifies phosphorylation of Ser^{893} in CARD11

To identify CARD11 phosphorylation sites, we used Jurkat T cells expressing wild-type (WT) CK1α or a form with a kinase-inactive D136N mutation (CK1α KI). CBM complex formation was abolished in CK1α knockout (KO) cells after PMA (phorbol 12-myristate 13-acetate)/ionomycin (P/I) stimulation, and reconstitution experiments demonstrated that this process depended on CK1α kinase activity (fig. S1, A to C). We enriched CARD11 protein by IP before digestion, peptide purification, and high-resolution, label-free liquid chromatography–MS/MS (LC-MS/MS) analyses, and the data from which were processed for peptide and phosphopeptide identification and quantification (*32*). Equivalent amounts of CARD11 protein were retrieved from all purifications (fig. S1D). We identified seven CARD11 phosphopeptides, composed of six phosphoserine and one phosphothreonine residue, with high probabilities and high phosphopeptide scores (Fig. 1A and data file S1). There are two possible start codons in the *CARD11* gene, which lead to the expression of a longer (1154 amino acids) or shorter (1147 amino acids) CARD11 protein, and we will use the official nomenclature of the longer CARD11 variant (fig. S1E). Identified phosphorylation sites localized between amino acids 439 to 925 in the CARD11 linker or MAGUK regions and the sites and surrounding sequences are evolutionarily highly conserved (Fig. 1B and fig. S1F). Constitutive phosphorylation of CARD11 was detected at Ser^{644}, Ser^{655}, Ser^{886}, and Ser^{925}, and P/I treatment enhanced phosphorylation at Ser^{439}, Thr^{654}, and Ser^{893} (Fig. 1C and fig. S1G). None of these phosphorylation events relied on CK1α kinase activity. Although phosphorylation at Ser^{644}, Ser^{886}, and Ser^{925} has been identified in large-scale phosphoproteomic studies (*30*, *31*), modifications at Ser^{439}, Thr^{654}, Ser^{655}, and Ser^{893} have not been previously identified as CARD11 phosphorylation sites.

A

CARD11 phosphosites NP001311210	CARD11 phosphosites EAL23962	Identified peptides	Localization probability	p-peptide score
Ser^{439}	Ser^{432}	RLpSKDSNNLDQSLPR	0.957934	109.72
Ser^{644}	Ser^{637}	FpSLERPFRPSVTSVGHVR	0.999796	88.872
Thr^{654}	Thr^{647}	PFRPSVpTSVGHVR	0.708518	50.158
Ser^{655}	Ser^{648}	PFRPSVTpSVGHVR	0.850051	56.514
Ser^{886}	Ser^{879}	NTLQPEEALSTSDPRVpSPR	0.999342	110.44
Ser^{893}	Ser^{886}	LSRApSFLFGQLLQFVSR	1	163.92
Ser^{925}	Ser^{918}	IISGpSPLGSLAR	0.998907	102.65

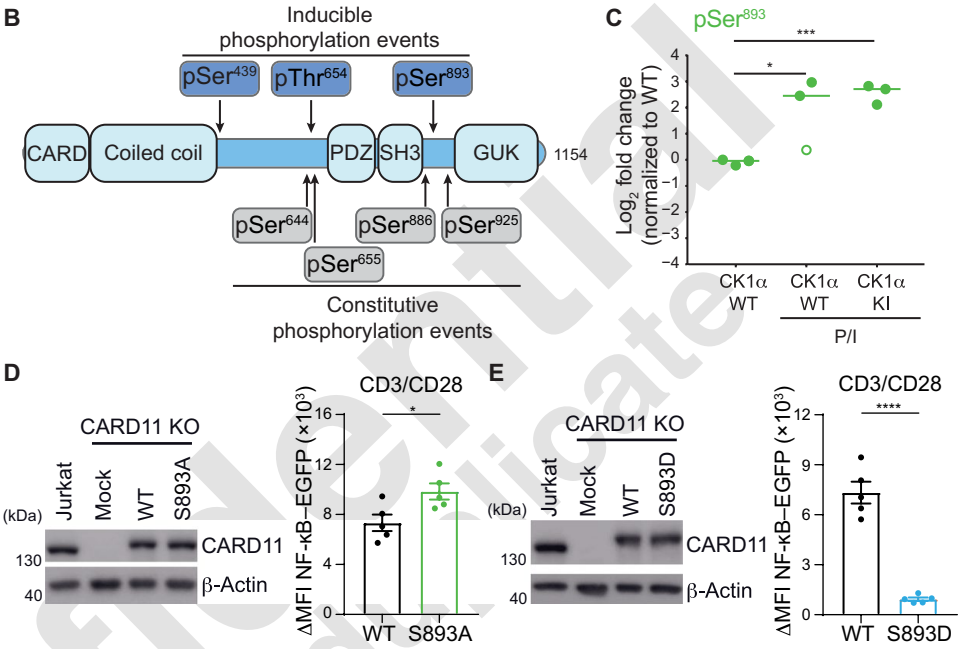

Fig. 1. Identification of inducible CARD11 Ser^{893} phosphorylation. (**A**) Overview of the CARD11 phosphorylated peptides identified by IP-LC-MS/MS in Jurkat T cells. Positions of phosphoserine/threonine residues according to the two CARD11 nomenclatures are indicated. (**B**) Domain structure and pictorial representation of phosphorylation sites identified in human CARD11. (**C**) The $\log_2$ fold changes assessed by LC-MS/MS analysis of the Ser^{893} phosphorylation site in untreated or P/I-treated (20 min) Jurkat T cells expressing CK1α WT or CK1α KI (kinase inactive). Unfilled circle indicates imputed value. Data are means of three biological replicates. Significance was determined by unpaired Student's *t* test comparing the difference between the means of two unmatched groups with the SEs of the difference. $^{*}P \leq 0.05$ and $^{***}P \leq 0.001$. (**D** and **E**) In Jurkat CARD11 KO NF-κB–EGFP reporter cells transduced with CARD11 S893A (D) or S893D (E), protein expression was analyzed by Western blot and NF-κB activation was determined by normalizing the median fluorescence intensity (MFI) after CD3/CD28 stimulation to that in unstimulated cells. Data are means ± SEM of five biological replicates. Significance was determined by unpaired Student's *t* test. $^{*}P \leq 0.05$ and $^{****}P \leq 0.0001$.

and phosphomutant constructs at close to endogenous levels (Fig. 1D and fig. S2, C to G). Ablation or mutations in CARD11 did not affect NF-κB activation in response to tumor necrosis factor α (TNFα). Although CARD11 S439A, T654A, or S655A mutations did not significantly affect NF-κB activation, rescue with the phosphodefective CARD11 S893A mutant augmented NF-κB reporter gene activation upon TCR/CD28 costimulation (Fig. 1D and fig. S2, C to E). Conversely, reconstitution of CARD11 KO Jurkat T cells with the phosphomimetic CARD11 S893D mutant severely compromised NF-κB activation after TCR/CD28 costimulation (Fig. 1E).

We used parental and CARD11 KO Jurkat T cells expressing an NF-κB–enhanced green fluorescent protein (EGFP) reporter gene (*13*, *28*) to detect changes in NF-κB activation upon CD3/CD28 or P/I stimulation (fig. S2, A and B). We characterized the newly identified and inducible phosphorylation events in cells with homogeneous lentiviral transduction and expression of Flag-StrepII CARD11 WT

To investigate the dynamics of CARD11 Ser^{893} phosphorylation, we generated a mouse monoclonal antibody that specifically recognized this phosphorylation (clone 25B10). This antibody recognized CARD11 WT, but not the S893A mutant, after pulldown of Flag-StrepII–tagged CARD11 from P/I-stimulated cells, and the

detection was lost after λ-phosphatase treatment (fig. S2H). CARD11 phosphorylated at Ser^{893} was also detected directly in lysates of Jurkat T cells expressing CARD11 WT but not the S893A mutant (Fig. 2A). Consistent with the data obtained by MS, Ser^{893} phosphorylation was increased (~4- to 6-fold) after 15 min of CD3/CD28 or P/I stimulation (Fig. 2, B and C). In Jurkat T cells, CARD11 Ser^{893} phosphorylation peaked within 5 to 30 min of CD3/CD28 or P/I stimulation and gradually decreased thereafter (Fig. 2, D and E). The onset of detectable CARD11 Ser^{893} phosphorylation preceded maximal IκBα or p65 phosphorylation. CARD11 Ser^{893} phosphorylation was induced by TCR ligation in the absence of the CD28 costimulus, which is necessary for robust IκBα degradation (Fig. 2F). CARD11 Ser^{893} phosphorylation was also induced after P/I stimulation and TCR or BCR crosslinking on primary murine and human T and B lymphocytes (Fig. 2, G to J, and fig. S2, I and J). Thus, CARD11 Ser^{893} phosphorylation is rapidly induced upon antigenic signaling in T and B cells.

CARD11 Ser^{893} phosphorylation controls the strength of NF-κB signaling in T cells

We directly compared the effects of CARD11 phosphodefective S893A and phosphomimetic S893D mutants on NF-κB activation and CBM complex signaling after reconstitution of CARD11 KO Jurkat T cells (Fig. 3A). Time-course analyses revealed that reconstitution with CARD11 S893A did not further enhance the robust NF-κB reporter gene activation in response to P/I stimulation but significantly augmented NF-κB activation between 2 and 6 hours after TCR/CD28 co-engagement or TCR ligation alone (Fig. 3, B and C, and fig. S3, A to D). Reconstitution with the phosphomimetic CARD11 S893D markedly reduced NF-κB activation at all time

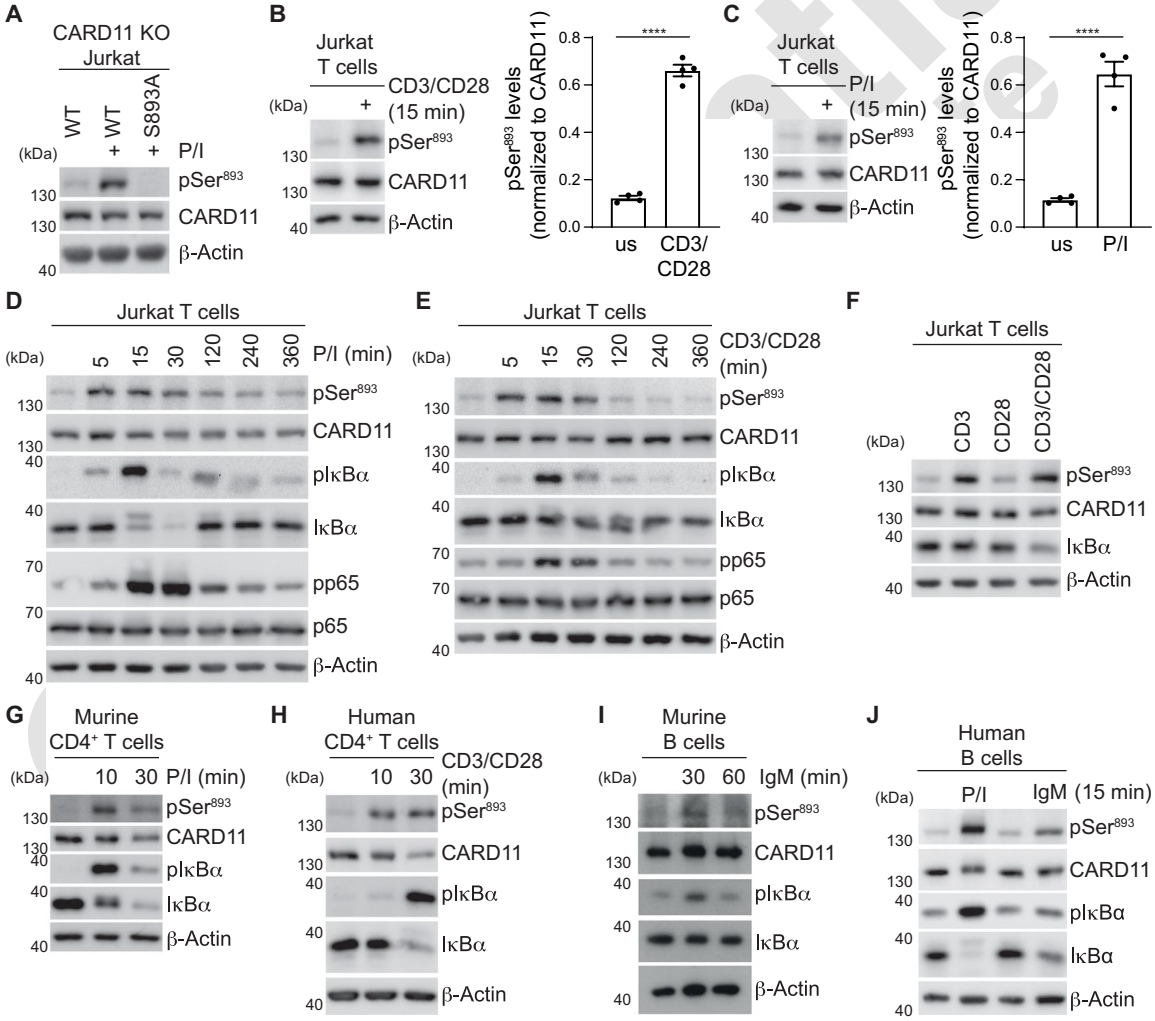

Fig. 2. Analyses of CARD11 Ser^{893} phosphorylation in lymphocytes. (**A**) Detection of phosphorylated Ser^{893} by Western blot analysis of P/I-stimulated CARD11 KO Jurkat T cells reconstituted with CARD11 WT or S893A. (**B** and **C**) Representative Western blot and quantification of CARD11 Ser^{893} phosphorylation after CD3/CD28 (B) or P/I (C) stimulation in Jurkat T cells. The phosphorylated Ser^{893} signal (normalized to total CARD11) was determined by densitometric analyses, and quantification of four biological replicates is shown. Significance was determined by unpaired Student's *t* test. $^{**}P \leq 0.01$ and $^{****}P \leq 0.0001$. us, unstimulated. (**D** and **E**) Kinetics of CARD11 Ser^{893} phosphorylation in Jurkat T cells after P/I (D) and CD3/CD28 (E) stimulation. The onset of NF-κB signaling was determined by IκBα phosphorylation/degradation and p65 phosphorylation. Representative of two biological replicates. (**F**) CARD11 Ser^{893} phosphorylation in Jurkat T cells after 20-min CD3, CD28, and CD3/CD28 stimulation. Representative of two biological replicates. (**G** to **J**) CARD11 Ser^{893} phosphorylation in primary murine CD4$^+$ T cells (G), human CD4$^+$ T cells (H), murine B cells (I), and human B cells (J) that were stimulated as indicated. Representative of two biological replicates.

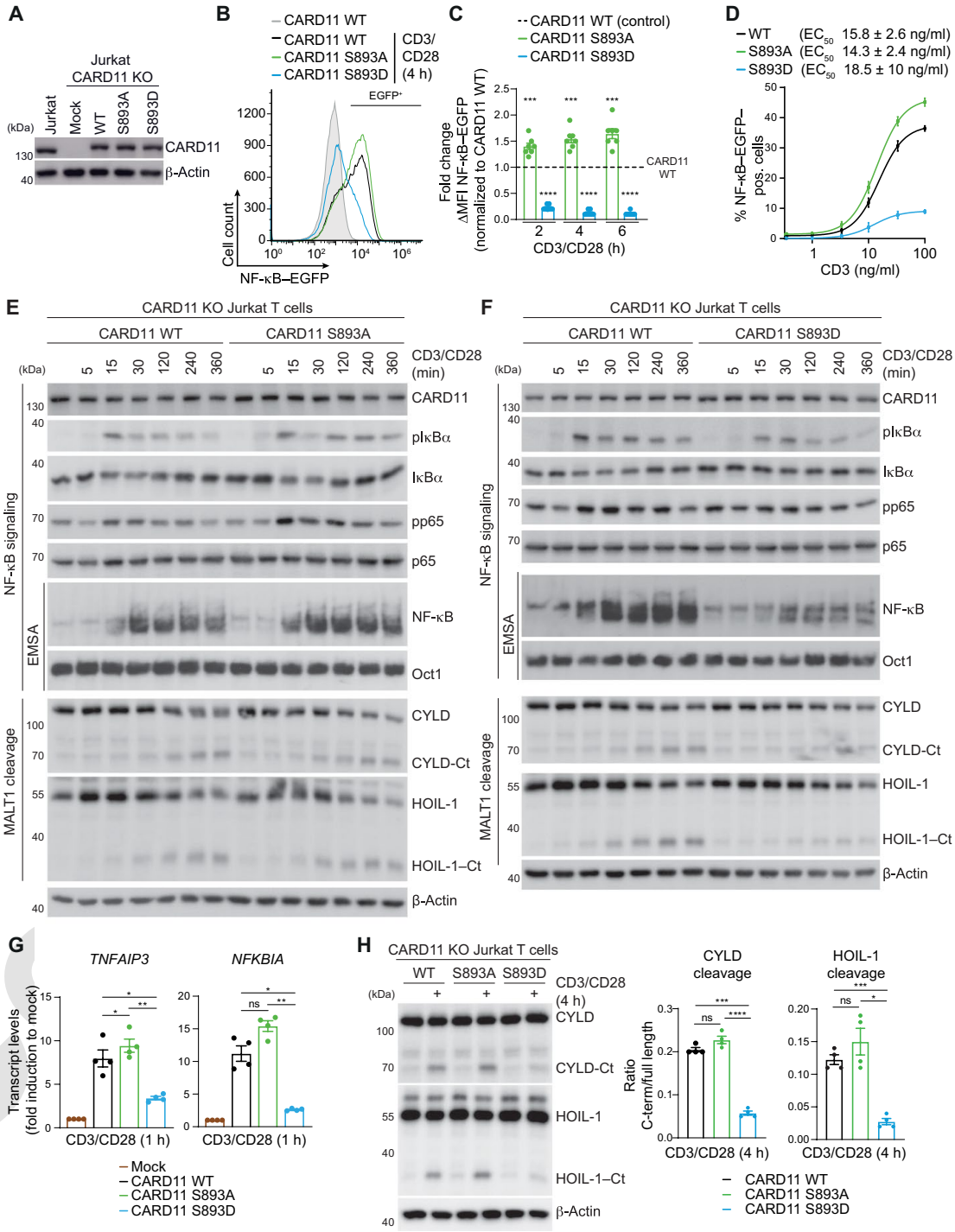

Fig. 3. Functional analyses of CARD11 Ser^{893} phosphorylation after reconstitution. (**A**) Expression of Flag-StrepII–tagged CARD11 constructs in CARD11 KO Jurkat T cells in comparison to parental Jurkat T cells by Western blot. (**B** and **C**) Induction of NF-κB–EGFP expression by flow cytometry following CD3/CD28 stimulation [(B), representative experiment] was quantified by determining the fold changes in median fluorescence intensity (MFI) of CARD11 WT-expressing cells (which was set as 1) and mutant-expressing cells over the indicated times (C). Data are means ± SEM of seven biological replicates. Significance was determined on $\log_2$ fold changes to normalized values by one-sample Student's *t* test. ***$P \leq 0.001$ and ****$P \leq 0.0001$. (**D**) Induction of NF-κB–EGFP reporter expression was measured after 4 hours of stimulation with increasing concentrations of anti-CD3 and constant amounts of anti-CD28 (1 μg/ml). NF-κB–EGFP–positive (pos.) cells were quantified, and EC_{50} values were determined. Data are means ± SEM of three biological replicates. (**E** and **F**) Effects of the expression of phosphodefective CARD11 S893A (E) and phosphomimetic CARD11 S893D (F) in reconstituted CARD11 KO Jurkat T cells on NF-κB signaling, DNA binding, and MALT1 protease activation after CD3/CD28 stimulation for the indicated times. Representative of two biological replicates. (**G**) Analyses of the induction of *TNFAIP3* and *NFKBIA* in CARD11 KO Jurkat T cells reconstituted with mock, CARD11 WT, CARD11 S893A, or CARD11 S893D stimulated with CD3/CD28 for 4 hours. Transcript levels in stimulated cells were normalized to those in mock-transfected cells. Data are means ± SEM of four biological replicates. Significance was determined with a one-way ANOVA combined with Tukey's multiple comparisons test. *$P \leq 0.05$ and **$P \leq 0.01$. ns, not significant. (**H**) Representative Western blot showing CYLD and HOIL-1 cleavage after 4 hours of CD3/CD28 stimulation of CARD11 KO Jurkat T cells reconstituted with CARD11 WT, S893A, or S893D. Quantification of the ratio of the cleavage products to full-length proteins after stimulation using densitometric analyses from four biological replicates. Significance was determined by one-way ANOVA combined with Tukey's multiple comparisons test. *$P \leq 0.05$, ***$P \leq 0.001$, and ****$P \leq 0.0001$. Ct, C terminus.

points and in response to all stimulatory conditions. Next, we titrated the amounts of anti-CD3 cross-linking antibodies while keeping the amounts of anti-CD28–activating antibodies constant (Fig. 3D). Whereas NF-κB transcriptional responses occurred at similar anti-CD3 concentrations [median effective concentration (EC_{50}), ~15 to 18 ng/ml], the amplitude of the NF-κB response was altered by expression of CARD11 WT, S893A, or S893D. Thus, early CARD11 Ser^{893} phosphorylation reduces the strength of NF-κB activation,

but it does not alter the sensitivity of the T cells to respond to TCR stimulation.

We tested how reconstitution with the CARD11 phosphomutants affected NF-κB and mitogen-activated protein kinase (MAPK) signaling and protease activation of MALT1 downstream of the CBM complex. Reconstitution with the phosphodefective CARD11 S893A mutant enhanced canonical NF-κB signaling after TCR/CD28 costimulation, as shown by the increases in IκBα phosphorylation and degradation, in p65 phosphorylation, and in NF-κB DNA binding (Fig. 3E). As expected from the reporter assays, the response to the strong P/I stimulus was mildly elevated by reconstitution with the phosphodefective CARD11 S893A mutant (fig. S4A). In contrast, reconstitution with the phosphomimetic CARD11 S893D mutant impaired NF-κB signaling and DNA binding in response to CD3/CD28 or P/I stimulation (Fig. 3F and fig. S4B). Consistent with these findings, CD3/CD28 induction of the NF-κB target genes *TNFAIP3* (TNFα-induced protein 3) and *NFKBIA* (NF-κB inhibitor α) was mildly enhanced or strongly diminished by reconstitution with the S893A or S893D mutants, respectively (Fig. 3G). Time-course analyses revealed that inducible MALT1 substrate cleavage was not notably altered in CARD11 S893A mutant-expressing Jurkat T cells but was reduced in CARD11 S893D mutant-expressing cells (Fig. 3, E and F, and fig. S4, A and B). Quantification of CYLD and HOIL-1 cleavage indicated that MALT1 protease activity was decreased by expression of the CARD11 S893D variant (Fig. 3H and fig. S4C). In addition, JNK phosphorylation was increased and decreased in CARD11 S893A– and CARD11 S893D-expressing Jurkat T cells, respectively, whereas extracellular signal–regulated kinase (ERK) phosphorylation was unchanged (fig. S5, A to D). Thus, inducible CARD11 Ser^{893} phosphorylation inhibits TCR signaling by impairing NF-κB, JNK, and MALT1 activation downstream of the CBM complex.

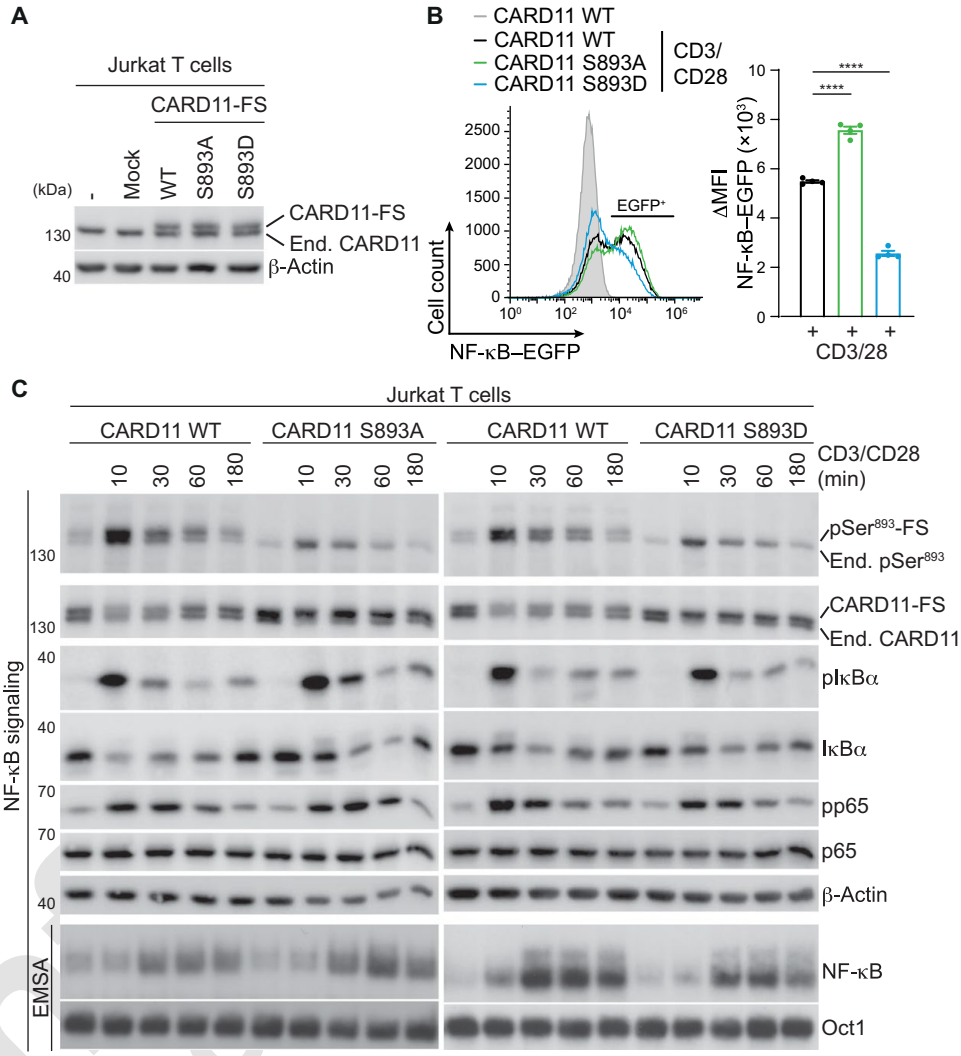

Fig. 4. Functional analyses of CARD11 Ser^{893} phosphorylation after overexpression. (**A**) Expression of Flag-StrepII (FS)–tagged CARD11 WT, S893A, and S893D in Jurkat T cells as determined by Western blot analysis. End., endogenous. (**B**) Induction of NF-κB–EGFP expression as determined by flow cytometry in Jurkat T cells stimulated with anti-CD3/CD28 (4 hours). NF-κB reporter gene activation was quantified by determining the fold changes in MFI of CARD11 WT- and mutant-expressing cells. Data are means ± SEM of four biological replicates. Significance was analyzed by one-way ANOVA combined with Dunnett's multiple comparisons test. ****$P \leq 0.0001$. (**C**) Effects of the expression of CARD11 WT, phosphodefective CARD11 S893A, or phosphomimetic CARD11 S893D on NF-κB signaling pathway activity in Jurkat T cells stimulated with CD3/CD28 for the indicated times. Representative of two biological replicates. EMSA, electrophoretic mobility shift assay.

To determine whether the extent of phosphorylation can tune T cell activation, we overexpressed CARD11 WT, S893A, and S893D in Jurkat T cells in the presence of endogenous CARD11. Viral transduction led to similar expression of exogenous Flag-StrepII–tagged CARD11 WT, S893A, or S893D in a ~50:50 ratio with endogenous CARD11 (Fig. 4A and fig. S6A). NF-κB activation in response to TNFα stimulation was not altered by expression of the mutants (fig. S6, B and C), whereas NF-κB reporter gene activation after TCR/CD28 costimulation was augmented by expression of the phosphodefective CARD11 S893A and reduced by that of the phosphomimetic CARD11 S893D (Fig. 4B). As expected, TCR/CD28-inducible Ser^{893} phosphorylation of endogenous or transduced CARD11 WT, but not those of the Ser^{893} mutants, was detected (Fig. 4C). Expression of CARD11 S893A was augmented, whereas CARD11 S893D counteracted NF-κB signaling and DNA binding in the presence of endogenous CARD11 in Jurkat T cells (Fig. 4C). Thus, increased CARD11 Ser^{893} phosphorylation affects NF-κB activation in a dominant-negative manner, showing that the extent of Ser^{893} phosphorylation tunes the strength of CARD11 signaling upon TCR/CD28 stimulation.

CARD11 Ser^{893} phosphorylation controls CBM-mediated survival signaling in lymphoma cells

To address the functional relevance of CARD11 Ser^{893} phosphorylation in B cells, we transduced NF-κB–EGFP reporter and CARD11 KO BJAB B cells and achieved homogeneous transduction and equivalent expression of CARD11 constructs. However, transduction yielded CARD11 overexpression compared to the amount of endogenous CARD11 parental BJAB cells (fig. S7, A and B), unlike in Jurkat T cells. NF-κB activity in response to lipopolysaccharide (LPS) stimulation, which does not require the CBM, was not affected by expression of the CARD11 phosphomutants (fig. S7C). The strong NF-κB reporter induction in CARD11 WT cells was not significantly increased in CARD11 S893A mutant cells, but NF-κB activation was nearly abolished by expression of the phosphomimetic CARD11 S893D mutant after P/I stimulation (Fig. 5A). P/I-induced NF-κB signaling was elevated and impaired in BJAB B cells reconstituted with the CARD11 S893A and S893D mutants, respectively (Fig. 5B). Further, expression of CARD11 S893A enhanced and that of CARD11 S893D reduced the cleavage of MALT1 substrates, which was confirmed by quantifying the ratio of cleaved to full-length HOIL-1 (Fig. 5C). Thus, Ser^{893} phosphorylation of CARD11 inhibits CBM-dependent events in B cells.

Because oncogenic CARD11 mutations bypass BCR upstream signaling to drive survival of diffuse large B cell lymphoma (DLBCL) cells (*33*), we assessed whether constitutive NF-κB activation by oncogenic CARD11 relies on Ser^{893} phosphorylation. We transduced CARD11 KO BJAB B cells containing the NF-κB–EGFP reporter with oncogenic CARD11 L232LI bearing the C-terminal S893A or S893D mutations (fig. S7, D and E). Neither the phosphodefective nor the phosphomimetic CARD11 Ser^{893} mutants altered constitutive NF-κB reporter gene activity or MALT1 substrate cleavage by reconstitution with oncogenic CARD11 L232LI (Fig. 5D and fig. S7E). Moreover, CARD11 Ser^{893} phosphorylation was not induced by expression of CARD11 L251P or L232LI, and the oncogenic mutants even suppressed CARD11 Ser^{893} phosphorylation after P/I stimulation, suggesting that oncogenic CARD11 activation impedes and bypasses the impact of the C-terminal phosphorylation (Fig. 5E). Expression of the BENTA (B cell expansion with NF-κB and T cell anergy) variant CARD11 E134G and the hypomorphic dominant-negative mutation CARD11 L194P caused a similar decrease in inducible phosphorylation at Ser^{893} (fig. S7F) (*34*, *35*). The decrease was more robust in BJAB B cells compared to that in Jurkat T cells, in which expression of CARD11 E134G, L194P, or L251P only slightly reduced Ser^{893} phosphorylation in response to P/I or CD3/CD28 stimulation (fig. S7, G and H). In BJAB B cells, CARD11 L232LI inhibited Ser^{893} phosphorylation in endogenous CARD11, showing that CARD11 oncogenic driver mutations can impair this inhibitory phosphorylation event in cis or trans (Fig. 5F). Compared to activated Jurkat T cells, neither activated B cell–type (ABC) nor germinal center B cell–type (GCB) DLBCL cell lines displayed increased Ser^{893} phosphorylation, despite the addiction to oncogenic lesions in BCR signaling components and chronic CBM complex assembly in ABC DLBCL cell lines (Fig. 5G). CARD11 Ser^{893} phosphorylation was induced by anti–immunoglobulin M (IgM) stimulation in SUD-HL6 cells and was sensitive to the Bruton's tyrosine kinase (BTK) inhibitor ibrutinib (Fig. 5H). Thus, acute, but not chronic, BCR signaling can induce CARD11 Ser^{893} phosphorylation in DLBCL cells.

We determined the influence of CARD11 Ser^{893} phosphorylation on signaling and proliferation of the ABC DLBCL cell line HBL1, which carries an activating mutation in the BCR adaptor CD79B that drives BCR survival signaling through the CBM complex (*36*). Lentiviral transduction of CARD11 WT, S893A, S893D, or L232LI yielded homogeneous transduction and expression in HBL1 cells (Fig. 5I and fig. S7I). The expression of CARD11 S893D was consistently slightly below that of the other CARD11 proteins, suggestive of a counterselection against the phosphomimetic mutant. Expression of oncogenic CARD11 L232LI enhanced CBM complex activity, as shown by augmented p65 phosphorylation and MALT1 protease activity and insensitivity of CBM activation to BTK inhibition by ibrutinib (Fig. 5I). Although the expression of CARD11 S893D was less compared to that of WT or S893A, its expression reduced p65 phosphorylation and impaired constitutive MALT1 substrate cleavage. CARD11 mutants did not alter overall HBL1 cell viability and proliferation (fig. S7J). We assessed the viability of HBL1 cells expressing CARD11 WT and mutants after treatment with the BTK inhibitor ibrutinib and the MALT1 inhibitor (S)-mepazine, both of which are toxic to ABC DLBCL cells (Fig. 5J and fig. S7K) (*37*, *38*). As predicted, expression of CARD11 L232LI protected HBL1 cells from cytotoxicity induced by ibrutinib, but not from that induced by (S)-mepazine. In contrast, expression of the CARD11 S893D mutant rendered HBL1 cells more sensitive to BTK inhibitor treatment but did not affect the response to downstream MALT1 inhibition. Thus, CARD11 Ser^{893} phosphorylation status can affect CBM complex activity in B cell lymphomas and can modulate the sensitivity of ABC DLBCL cells to inhibitors that target BCR upstream signaling.

PKCθ-catalyzed CARD11 Ser^{893} phosphorylation impairs CBM complex formation

CARD11 Ser^{893} is rapidly phosphorylated after T cell stimulation, and phosphosite predictions revealed that Ser^{893} in CARD11 localizes to a putative consensus motif for phosphorylation by novel PKC isoforms (fig. S8A). In Jurkat T cells, the PKCθ-selective inhibitor AEB071 (also known as sotrastaurin) (*39*, *40*) efficiently inhibited inducible CARD11 Ser^{893} phosphorylation at a concentration sufficient for abolishing canonical NF-κB signaling (Fig. 6A and fig. S8B). Further, recombinant PKCθ catalyzed phosphorylation at Ser^{893} in a CARD11 peptide (amino acids 885 to 901) comprising the PKC phosphoconsensus site Ser^{893} in an in vitro kinase reaction, demonstrating that PKCθ can function as the kinase that phosphorylates this site (Fig. 6B). We determined whether CARD11 Ser^{893} was phosphorylated in Jurkat T cells deficient for MALT1, BCL10, or CK1α, which are all critical for efficient CBM complex assembly (*12*, *28*). MALT1, BCL10, or CK1α deficiency prevented NF-κB signaling but did not impair CARD11 Ser^{893} phosphorylation (Fig. 6C and fig. S8C). To investigate whether Ser^{893} phosphorylation occurs within or outside of the CBM complex, we performed size exclusion chromatography (SEC) to detect the high–molecular weight CBM complex after stimulation (*41*). In extracts of CARD11 WT-containing Jurkat T cells, CARD11 phosphorylated at Ser^{893} comigrated with free, CBM-unbound CARD11 (fractions 14 to 18), but not with CARD11 in the higher-order CBM complex (fractions 6 to 9) after P/I stimulation (Fig. 6D and fig. S8D). Thus, CBM complex formation is not obligatory for PKCθ-driven Ser^{893} phosphorylation, and the majority of CARD11 phosphorylated at Ser^{893} does not appear to be integrated into the CBM complex.

To explore the impact of Ser^{893} modification on the CARD11 interactome, we performed MS after pulldown of Flag-StrepII–tagged WT or mutant CARD11 from Jurkat T cells. CARD11 WT

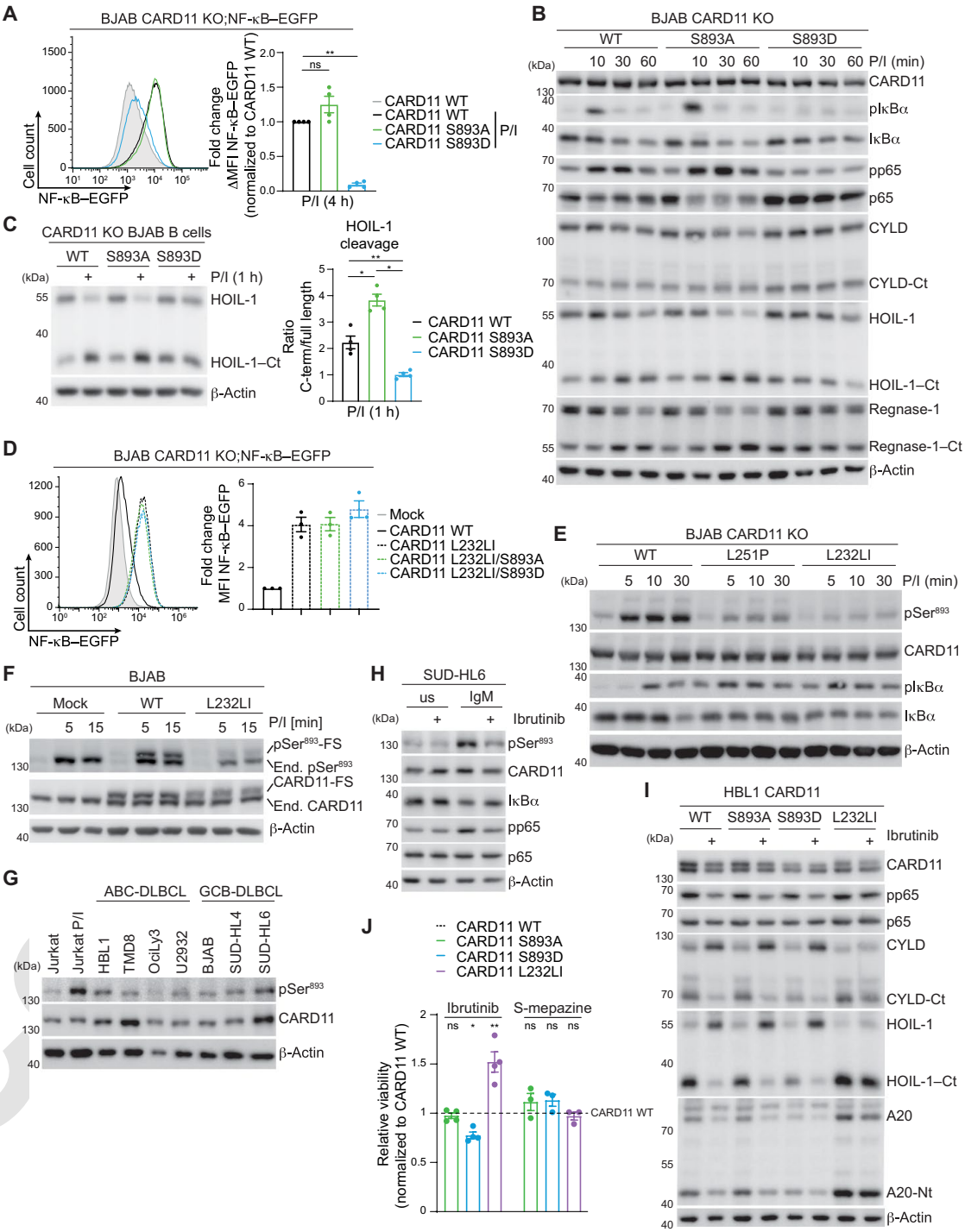

Fig. 5. CARD11 Ser^{893} phosphorylation suppresses acute and chronic CBM complex in B cells. (**A**) NF-κB–EGFP induction was determined by flow cytometry in CARD11 KO BJAB B cells reconstituted with CARD11 WT, S893A, or S893D following P/I stimulation (4 hours). NF-κB–EGFP expression was quantified by normalizing the MFI of mutant-expressing cells to the MFI of CARD11 WT-expressing cells. Data are means ± SEM of four biological replicates. Significance was determined on $\log_2$ fold changes to normalized values by one-sample Student's *t* test. $^{**}P \leq 0.0001$. (**B**) Effects of the reconstitution of CARD11 KO BJAB B cells with the phosphodefective CARD11 S893A or phosphomimetic CARD11 S893D mutants on NF-κB signaling and MALT1 protease activation after P/I stimulation for the indicated times. Representative of two biological replicates. (**C**) Representative Western blot showing HOIL-1 cleavage after 1 hour of P/I stimulation in CARD11 KO BJAB B cells reconstituted with CARD11 WT, S893A, or S893D. Quantification of the ratio of the cleavage product to full-length HOIL-1 after stimulation using densitometric analyses from four biological replicates. Significance was determined by a one-way ANOVA combined with Tukey's multiple comparisons test. $^{*}P \leq 0.05$ and $^{**}P \leq 0.01$. (**D**) NF-κB–EGFP induction in CARD11 KO NF-κB–EGFP reporter BJAB cells reconstituted with CARD11 L232LI, L232LI/S893A, or L232LI/S893D mutants was analyzed by flow cytometry. Data are means ± SEM of three biological replicates comparing fold change in the MFIs of CARD11 WT- and mutant-expressing cells . (**E**) CARD11 Ser^{893} phosphorylation was determined in CARD11 KO BJAB cells reconstituted with CARD11 WT or oncogenic CARD11 L251P or L232LI mutants before or after P/I stimulation. Representative of two biological replicates. (**F**) Ser^{893} phosphorylation of endogenous and overexpressed CARD11 WT or L232LI was determined in BJAB cells before or after P/I stimulation. Representative of three biological replicates. (**G**) CARD11 Ser^{893} phosphorylation was determined in four ABC and three GCB DLBCL cell lines by Western blot. Representative of two biological replicates. (**H**) Induction of CARD11 Ser^{893} phosphorylation in SUD-HL6 cells in response to IgM (15 min) and sensitivity to ibrutinib treatment. Representative of three biological replicates. (**I**) Effects of CARD11 WT, S893A, S893D, or L232LI expression in HBL1 cells on p65 phosphorylation and MALT1 substrate cleavage without or with ibrutinib treatment (18 hours) were assessed by Western blot. Representative of two biological replicates. (**J**) Effects of CARD11 WT, S893A, S893D, or L232LI expression on HBL1 cell proliferation in the absence or presence of ibrutinib or S-mepazine treatment. The changes in the relative viability of mutant-expressing cells normalized to that of CARD11 WT-expressing cells after 4 days of inhibitor treatment are shown. Data are means ± SEM of four (ibrutinib) or three (S-mepazine) biological replicates. Significance was determined on $\log_2$ fold changes to normalized values by one-sample Student's *t* test. $^{*}P \leq 0.05$ and $^{**}P \leq 0.01$.

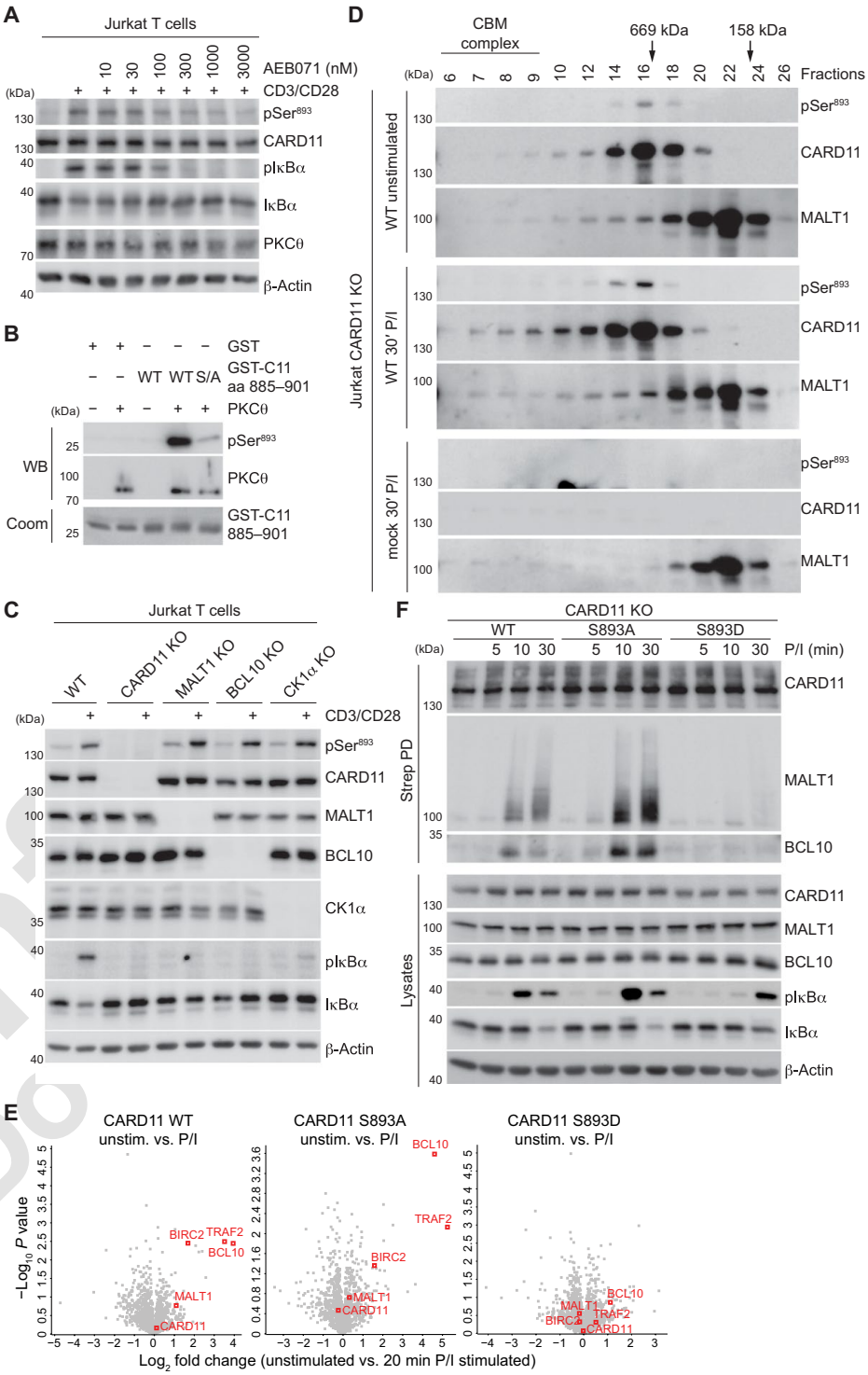

Fig. 6. PKCθ-catalyzed CARD11 Ser^{893} phosphorylation counteracts CBM complex formation. (**A**) Inhibition of CARD11 phosphorylation on Ser^{893} induced by CD3/CD28 stimulation by increasing concentrations of the PKCθ inhibitor AEB071 was assessed by Western blot. Representative of two biological replicates. (**B**) In vitro PKCθ kinase assay on GST-tagged CARD11 peptide [amino acids (aa) 885 to 901] was followed by detection of CARD11 phosphorylation on Ser^{893} by Western blotting and Coomassie staining. Representative of two biological replicates. (**C**) Jurkat T cells with KOs of the indicated CBM component were stimulated with CD3/CD28 (20 min), and CARD11 Ser^{893} phosphorylation and IκBα phosphorylation/degradation were assessed by Western blot. Representative of two biological replicates. (**D**) Co-elution of Ser^{893} phosphorylated CARD11 with the CBM-unbound CARD11 was analyzed by SEC in lysates of CARD11 KO Jurkat T cells reconstituted with CARD11 WT or mock-transduced. Western blot shows fractions of CARD11 phosphorylated at Ser^{893} and CBM complex (CARD11/MALT1 comigration) after SEC of CARD11 WT cells unstimulated (top panels) or P/I-stimulated (middle panel). P/I-stimulated mock-transduced cells show lack of MALT1 migration to CBM fractions in the absence of CARD11 (bottom panels). Peak elutions of CBM complex and molecular weight standards are shown at the top. Representative of two biological replicates. (**E**) Enrichment of proteins bound to Flag-StrepII–tagged CARD11 WT, S893A, and S893D after streptavidin pulldowns of lysates of Jurkat T cells by LC-MS/MS analysis. Volcano plots show protein enrichment ($\log_2$ fold change) and significance ($-\log_{10} P$ values) calculated for each protein bound to CARD11 WT, S893A, and S893D before and after 20-min P/I stimulation from three biological replicates as depicted. (**F**) CBM complex formation after P/I stimulation (5, 10, or 30 min) was analyzed after streptavidin pulldowns (PD) of Flag-StrepII–tagged CARD11 WT, S893A, or S893D from reconstituted CARD11 KO Jurkat T cells using Western blot. Representative of two biological replicates.

and S893A, but not S893D, recruited BCL10 after P/I stimulation (Fig. 6E and fig. S8E). Similarly, P/I induced the recruitment of TNF receptor–associated factor 2 (TRAF2) and baculoviral IAP repeat containing 2 (BIRC2; also known as CIAP1) to CARD11 WT and S893A, but not to S893D. We did not detect significant changes in the binding of other non-CBM–related interaction partners to CARD11 S893D (data file S2), suggesting that the primary function of the C-terminal phosphorylation was to prevent CBM complex formation. To confirm the impact of CARD11 Ser^{893} phosphorylation on CBM complex assembly, we performed Western blotting after pulldown of Flag-StrepII–tagged WT or mutant CARD11 from Jurkat T cells (Fig. 6F and fig. S8, F and G). Whereas the association of BCL10, ubiquitinated MALT1, and TRAF2 after P/I stimulation was enhanced in cells expressing the phosphodefective CARD11 S893A mutant, expression of the phosphomimetic CARD11 S893D nearly abolished inducible binding of these factors. We compared the effects of the phosphomutants to the N-terminal CARD11 R42A mutant, which cannot mediate heterotypic CARD-CARD interaction between CARD11 and BCL10 (*42*). Expression of the CARD11 S893D or R42A mutants also decreased BCL10, MALT1,

and TRAF2 binding, revealing that phosphorylation in the CARD11 MAGUK region affects the CBM holo-complex in a manner that is as severe as a destructive mutation in the CARD of CARD11 (fig. S8G). Thus, PKC-catalyzed phosphorylation on Ser^{893} in the CARD11 C terminus is a potent inhibitory signal that suppresses CBM complex assembly and thereby counteracts lymphocyte activation.

DISCUSSION

Ser^{893} phosphorylation maintains CARD11 in the inactive conformation, whereas unmodified Ser^{893} facilitates an active state, which is required to recruit BCL10-MALT1 dimers upon stimulation (*14*). The C-terminal MAGUK region is critical for CARD11 activity and CBM complex assembly (*43*–*46*), and our data demonstrate that posttranslational modifications in the C terminus are critical in controlling CARD11 scaffolding functions. Ser^{893} is located in a region termed the hook domain, which has been suggested to stabilize CARD11 (*45*), but we did not find evidence that Ser^{893} phosphorylation altered CARD11 stability. Structural modeling has indicated that the hinge region between the SH3 and GUK domains is unstructured and that its deletion impairs intramolecular and favors intermolecular SH3-GUK associations (*43*). Ser^{893} phosphorylation in the hinge region may hinder the switch from an inactive intramolecular to an active intermolecular assembly of CARD11, which causes CARD11 oligomerization and BCL10-MALT1 filament formation (*10*–*12*, *43*). Structural analysis of the CARD11 C terminus will be required to determine the exact influence of the hinge region and Ser^{893} phosphorylation on CBM complex assembly.

Phosphodefective S893A acted like a gain-of-function (GOF) CARD11 variant after stimulation, but it was not sufficient to trigger constitutive CARD11 activity, as observed for the oncogenic or BENTA mutations (*2*, *9*). In contrast, phosphomimetic CARD11 S893D acted like a dominant-negative loss-of-function (LOF) mutant that suppressed acute or chronic NF-κB and MALT1 protease activation in T cells or lymphoma cells (*9*, *47*). Thus, the level of CARD11 Ser^{893} phosphorylation can tune response magnitude. Of note, the lack of increased Ser^{893} phosphorylation after chronic BCR signaling or expression of BENTA- and DLBCL-derived CARD11 GOF mutants suggested that oncogenic mechanisms may bypass the dominant-negative effect of this modification to allow the survival and growth of lymphoma cells. CARD11-activating mutations can even impede the inhibitory Ser^{893} phosphorylation of CARD11 WT in trans, which may at least partially explain the strong oncogenic potential of the CARD11-activating mutants in a heterozygous setting (*33*). Further, a dominant-negative CARD11 L194P mutant derived from a CADINS (CARD11-associated atopy with dominant interference of NF-κB signaling) patient also suppressed Ser^{893} phosphorylation. The CARD11 L194P mutation abolishes CBM complex formation, and its dominant-negative effect may disconnect CARD11 from both positive and negative upstream regulators (*34*). Of note, the counterbalancing effect of the GOF or LOF mutants on Ser^{893} phosphorylation was more pronounced in BJAB B cells than in Jurkat T cells. Whether differences in neutralizing the inhibitory Ser^{893} phosphorylation may account for some differential responses, such as of the BENTA mutants in T and B cells, will need further investigation (*35*). Our current analyses on the impact of CARD11 mutants is limited by available cell line models, and it will be interesting to study the level and impact of Ser^{893} phosphorylation in lymphocytes from CARD11-mutant BENTA or CADINS patients.

As observed for the activating CARD11 phosphorylation of Ser^{559} and Ser^{652} (*19*–*21*), PKCθ also catalyzes the inhibitory Ser^{893} phosphorylation in T cells. Kinases downstream of PKCθ may be involved, but the rapid parallel onset of activating and inhibiting modifications after TCR/CD28 ligation suggest that similar or identical pathways are operational (*23*, *28*). Thus, PKCθ has two opposing functions for lymphocyte activation, and we showed that the level of inhibitory Ser^{893} phosphorylation affected the strength of the TCR response. We showed that Ser^{893} phosphorylation affected T cell activation in two ways. First, anergic TCR stimulation alone triggered Ser^{893} phosphorylation without a costimulus. Thus, phosphorylation of Ser^{893} may raise the threshold for signaling to occur and thereby prevent T cell activation from tonic signaling in resting cells or in the absence of costimulation in anergic cells (*48*). Second, the inhibitory effect of PKCθ-mediated Ser^{893} phosphorylation may facilitate the switch-like activation of the CARD11 scaffold (*22*). PKCθ/β alone is not sufficient to trigger CBM complex activation, and a positive feedback loop is required, in which the downstream kinase IKKβ phosphorylates additional residues in CARD11 (*22*–*24*). Although PKC-catalyzed Ser^{893} phosphorylation will favor the inactive "off" state of CARD11 in T cells prone to tonic or anergic TCR stimulation without a costimulus, the combined action of PKCθ and IKKβ after costimulation will shift signaling toward activating kinases that foster CBM assembly and activity. The inhibitory Ser^{893} CARD11 phosphorylation occurs within minutes after antigenic stimulation. Similar kinetics have been described for stimulatory CARD11 phosphorylation events (*20*, *23*, *28*). It will be necessary to delineate the interdependency and exact chronologic order of these stimulatory and inhibitory modifications, but now we are limited by a lack of antibodies that recognize the stimulatory phosphorylation events. In other systems, the combined action of positive and negative regulators can generate robust responses in a multistable system (*49*). A similar scenario has been proposed for CK1α, whose catalytic activity is required for CBM assembly, but Ser^{615} phosphorylation of CARD11 by CK1α also suppresses NF-κB activation (*27*, *28*). By these mechanisms, stimulatory and inhibitory CARD11 phosphorylation events can cooperate to set signaling thresholds and to shape the dynamics of CBM complex assembly, which orchestrates lymphocyte activation. Understanding the mechanisms that regulate CARD11 may guide strategies for improving therapeutic T cell responses for the treatment of immune diseases and cancer.

MATERIALS AND METHODS

Cell culture

Human embryonic kidney (HEK) 293T cells were cultured in Dulbecco's modified Eagle's medium [with 10% fetal bovine serum (FBS) and penicillin/streptomycin (P/S; 100 U/ml)] and were passaged upon reaching 80% confluency. Cells were trypsinized (0.05% trypsin/EDTA) and then seeded at the appropriate density for experiments. Jurkat T cells and BJAB B cells (including all KO and reconstituted cells) were cultured in RPMI 1640 [with 10% FBS and P/S (100 U/ml)]. Generation of CARD11, MALT1, BCL10, and CK1α KO Jurkat T cells and CARD11 KO BJAB B cells has been described previously (*12*, *13*, *28*, *50*). DLBCL cell lines (HBL1, TMD8, OciLy3, U2932, SUD-HL4, and SUD-HL6) were cultured in RPMI 1640 [with 15% FBS and P/S (100 U/ml)]. Suspension cell lines were maintained at a density of 0.5×10^6 to 1.5×10^6 cells/ml. AQ4

Cell lines were regularly checked for mycoplasma contamination. Primary murine splenocytes were isolated from spleen and treated with Red Blood Cell Lysis Solution (Miltenyi). Lymphocytes were purified using the Mouse CD4$^+$ T Cell Isolation Kit (Miltenyi) or the Mouse B Cell Isolation Kit using magnetic-activated cell sorting (MACS). Primary murine cells were suspended in RPMI 1640 containing 10% FBS (heat-inactivated), P/S (100 U/ml), 1% Hepes (pH 7.5), 2 mM L-glutamine, 1% minimum essential medium nonessential amino acids, 1 mM sodium pyruvate, and 50 μM β-mercaptoethanol at 2×10^6 cells/ml for treatment. Acquisition and isolation of primary human CD4$^+$ T cells and B cells from blood of donors were performed as previously described using the Human CD4$^+$ T Cell and Human B Cell Isolation Kit (Miltenyi) using MACS. Human CD4$^+$ T cells and B cells were suspended in T cell medium [RPMI 1640–10% FBS, P/S (100 U/ml), 50 μM β-mercaptoethanol] at a density of 2×10^6 cells/ml for treatment. Animal care was in accordance with institutional guidelines. Written consent and approval by the ethics board of the Medical Faculty at the Technical University Munich were obtained for the use of peripheral blood from healthy donors.

Cell stimulation and treatment

Cells were stimulated with P/I (200/300 ng/ml; Merck). Except when specified otherwise, anti-CD3/CD28 stimulation was performed using murine anti-human CD3 antibody (1 μg/ml) and murine anti-human CD28 antibody (3.3 μg/ml), in addition to anti-mouse IgG1 and anti-mouse IgG2a antibodies (1.6 μg/ml) in 300 μl of medium. Cells were stimulated with TNFα (20 ng/ml; Sigma-Aldrich) in 2 ml of medium and LPS (Sigma-Aldrich) at a concentration of 5 μg/ml. Inhibitors were dissolved in dimethyl sulfoxide, and cells were treated with 20 nM ibrutinib (LC Laboratories), 20 μM S-mepazine, and 10 nM to 3 μM ABE071 (Biozol). IgM stimulation of human and murine B cells was performed at 10 μg/ml with the appropriate goat anti-IgM (Jackson ImmunoResearch).

Generation of monoclonal antibodies against CARD11 Ser^{893} and MALT1

Mouse monoclonal antibodies against the CARD11 Ser^{893} phosphorylation site were generated by immunization of Balb/c mice with ovalbumin-coupled peptides comprising phosphorylated Ser^{893} (Peps 4LS, Heidelberg). Animals were injected subcutaneously and intraperitoneally with 40 μg of peptide, 5 nmol CpG (Tib Molbiol, Berlin, Germany), and an equal volume of incomplete Freund's adjuvant (IFA). Mice received a booster immunization without IFA after 11 weeks, and spleen cells were fused with P3X63Ag8.653 myeloma cells using standard procedures. Hybridoma supernatants were screened for binding to biotinylated phosphopeptides coupled to streptavidin beads (PolyAn Red4 Multiplex Beads, Berlin, Germany) in a multiplex flow cytometry immunoassay (iQue, Intellicyt; Sartorius, Göttingen, Germany). Specificity was confirmed by negative screening on the appropriate nonphosphorylated peptide. Positive supernatants were further validated by Western blot analysis using conditions used for phosphopeptide identification by LC-MS/MS. Hybridoma cells from selected supernatants were subcloned at least twice by limiting dilution to obtain stable monoclonal cell clones that recognize phosphorylated Ser^{893}. To verify phosphorylation, γ-phosphatase (160 U; New England Biolabs) was incubated for 30 min at 30°C after streptavidin pulldown of Flag-StrepII–tagged CARD11 before samples were analyzed by Western blot. Experiments in this work were performed with hybridoma supernatant CARP 25B10 (IgG2a/k).

Rat monoclonal antibodies against human MALT1 were generated by immunizing Wistar rats with 70 μg of recombinant MALT1 protein (amino acids 339 to 719). Hybridoma supernatants were generated as described above and screened for binding to or capturing of recombinant his-tagged MATL1 protein by binding or capture enzyme-linked immunosorbent assay, respectively. Positive supernatants were further validated by Western blot and IP assays. Hybridoma supernatant MLT1 17C11 (IgG2b/k) was used in this work for detection of MALT1 after SEC.

Lentiviral transduction

For stable expression of proteins, parental or KO cells were transduced with lentiviruses expressing pHAGE-hΔCD2-T2A-CARD11 or pHAGE-hΔCD2-T2A-CK1α WT or mutant constructs. The list of DNA constructs used is shown in table S1, and viral transduction was performed as previously described (*28*).

Western blotting and electrophoretic mobility shift assays

For NF-κB signaling, 1×10^6 to 3×10^6 Jurkat T cells were harvested (300*g*, 5 min, 4°C) and washed with phosphate-buffered saline (PBS) before being lysed in 60 to 120 μl of high-salt buffer [20 mM Hepes (pH 7.9), 350 mM NaCl, 20% (v/v) glycerol, 1 mM $MgCl_2$, 0.5 mM EDTA, 0.1 mM EGTA, 1% NP-40, 1 mM dithiothreitol (DTT), 10 mM NaF, 8 mM β-glycerophosphate, and 300 μM sodium vanadate] and protease inhibitor cocktail (Roche) for 20 to 60 min at 4°C. Lysates were cleared by centrifugation (20,000*g*, 15 to 60 min, 4°C). For MALT1 substrate cleavage, the same procedure was done with co-IP buffer [25 mM Hepes (pH 7.5), 150 mM NaCl, 1 mM glycerol, 0.2% NP-40 (v/v), 1 mM DTT, 10 mM NaF, 8 mM β-glycerophosphate, and 300 μM sodium vanadate] and protease inhibitor cocktail (Roche). Protocols for Western blotting and electrophoretic mobility shift assays were performed as previously described (*28*). Western blot images were recorded using the ECL ChemoCam Imager with the ChemoStar software and quantified using LabImage 1D L340 software (INTAS Science Imaging). Antibodies are listed in table S2.

Analyses of NF-κB target gene expression

Total RNA was prepared from 3×10^7 Jurkat T cells after stimulation with anti-CD3/CD28 (4 hours) using the RNeasy Mini Kit (74106, Qiagen). Reverse transcription (RT) of RNA into complementary DNA (cDNA) was performed using a Verso cDNA synthesis kit (AB1453B, Thermo Fisher Scientific). Quantitative RT-PCR (polymerase chain reaction) was performed using Takyon No ROX SYBR 2X MasterMix blue dTTP (UF-NSMTB0710, Eurogentec), and samples were measured on a Roche LightCycler 480 II instrument. RNA polymerase II (RPII) served as internal standard. The following primers were used: RPII [5′-GTTCGGAGTCCTGAGTCCGGATG-3′ (forward) and 5′-CCTGCCTCGGGTCCATCAGC-3′ (reverse)], TNFAIP3 [5′-CTGAAAACGAACGGTGACGG-3′ (forward) and 5′-CGTGTGTCTGTTTCCTTGAGCG-3′ (reverse)], and NFKBIA [5′- AGGACGGGGACTCGTTCCTG-3′ (forward) and 5′-CAAGTGGAGTGGAGTCTGCTG-3′ (reverse)].

Protein interaction studies

Cells (3×10^7 to 6×10^7) were lysed in 800 μl of co-IP buffer [25 mM Hepes (pH 7.5), 150 mM NaCl, 1 mM glycerol, 0.2% NP-40 (v/v), 1 mM DTT, 10 mM NaF, 8 mM β-glycerophosphate, and 300 μM

sodium vanadate] and protease inhibitor cocktail (Roche). Lysates were incubated with rotation (30 to 60 min at 4°C) and then centrifuged (20,000*g*, 20 min, 4°C). Aliquots of supernatant (input) were retained for Western blotting. For BCL10 co-IP, 0.5 μg of BCL10 antibody (C-17, Santa Cruz Biotechnology) was added and incubated with rotation overnight at 4°C. Protein G Sepharose 4B beads (25 μl; 1:1 suspension; Life Technologies) were added for 1 to 2 hours at 4°C. For streptavidin pulldowns, 30 μl of Strep-Tactin Sepharose (1:1 suspension, IBA) was added and rotated (overnight at 4°C). Beads were subsequently washed three times with 500 μl of ice-cold co-IP buffer without protease and phosphatase inhibitors (200*g*, 2 min, 4°C). The supernatant was removed, 15 to 25 μl of 2x SDS loading buffer (Roti-Load, Roth) were added, and the beads were boiled (95°C, 7 min) and then analyzed by Western blot.

Flow cytometry

To assess hΔCD2 surface expression of infected cells, approximately AQ8 0.2×10^6 cells were stained with anti-CD2–APC antibody (human; dilution, 1:400) for 15 to 20 min at 4°C in the dark. To assess NF-κB reporter gene activity by the EGFP reporter, 0.5×10^5 cells were stimulated as depicted in the figure legends. Cells were washed and resuspended in 300 μl of PBS and analyzed on Attune Acoustic Focusing Cytometer. Data analysis was performed with FlowJo software 10.7.1, either by gating the number or by calculating the mean fluorescence intensity (MFI) of the cells. Calculations of change in MFI (ΔMFI) were performed by normalization to WT control.

Liquid chromatography and tandem mass spectrometry

To identify CARD11 phosphosites, CK1α KO Jurkat T cells reconstituted with CK1α WT or D136N were used. Cells (6×10^7 per sample) were left untreated or stimulated for 20 min with P/I before lysis in 1% NP-40 buffer [150 mM NaCl, 50 mM tris-HCl (pH 7.5), 10 mM Na-pyrophosphate, 10 mM Na-glycerophosphate, 1% NP-40, 20 mM NaF, 1 mM EGTA, 1 mM EDTA, 1 mM DTT, 10% glycerol, and protease inhibitors]. CARD11 IP [anti-CARD11 N20 (3 μg per sample), sc-20458] was performed overnight, and binding to protein G Sepharose 4B beads (Life Technologies) was performed for 2 hours at 4°C. To identify interactors of C-terminal Flag-StrepII–tagged CARD11 WT, S893A, or S893D, cells were left untreated or stimulated for 20 min with P/I and streptavidin pulldowns were performed as described earlier using CARD11 KO Jurkat T cells reconstituted with the respective CARD11 constructs (6×10^7 cells per sample). After IPs or pulldowns, beads were washed twice in 1% NP-40 buffer and twice in 50 mM tris-HCl (pH 7.5) buffer before resuspending in 50 mM tris-HCl (pH 7.5) buffer to perform overnight on-bead digestion at 37°C using trypsin in 2 M urea [dissolved in 50 mM tris-HCl (pH 7.5)]. The resulting peptides were purified using in-house prepared SDB-RPS (Empore) stage tips (*51*) before LC-MS/MS analysis as described previously (*52*).

For sample analysis after CARD11 IPs, peptides were separated on a 50-cm reversed-phase column [75 μm inner diameter, packed in-house with ReproSil-Pur C18-AQ 1.9 μm resin (Dr. Maisch GmbH)] with a binary buffer system of buffer A [0.1% formic acid (FA)] and buffer B (80% acetonitrile plus 0.1% FA) over 60-min gradient (5 to 30%, 30 to 60%, and 60 to 95% of buffer B for 40, 4, and 4 min, respectively, and 12-min wash time) using the EASY-nLC 1200 system (Thermo Fisher Scientific) with a flow rate of 300 nl/min. Column temperature was maintained at 60°C. The nLC system was coupled to a Q Exactive HF-X mass spectrometer (Thermo Fisher Scientific) that acquired full scans [300 to 1650 mass/charge ratio (m/z), maximum injection time of 20 ms, resolution of 60,000 at 200 m/z] at a target of 3×10^6 ions. The 10 most intense ions were AQ9 isolated and fragmented with higher-energy collisional dissociation (HCD) (target of 1×10^5 ions, maximum injection time of 60 ms, isolation window of 1.4 m/z, and NCE of 27%) and detected in the AQ10 Orbitrap (resolution of 15,000 at 200 m/z). Dynamic exclusion was set to 20 s. For streptavidin pulldowns of CARD11 WT, S893A, and S893D, peptides were separated on a 50-cm reversed-phase column [75 μm inner diameter, packed in-house with ReproSil-Pur C18-AQ 1.9 μm resin (Dr. Maisch GmbH)] with a binary buffer system of buffer A (0.1% FA) and buffer B (80% acetonitrile plus 0.1% FA) over 60-min gradient (5 to 30%, 30 to 65%, and 65 to 95% of buffer B for 35, 5, and 5 min, respectively, and 15-min wash time) using the EASY-nLC 1200 system (Thermo Fisher Scientific) with a flow rate of 300 nl/min. Column temperature was maintained at 60°C. The nLC system was coupled to an Orbitrap Exploris 480 mass spectrometer (Thermo Fisher Scientific) that acquired full scans (300 to 1650 m/z, maximum injection time of 25 ms, and resolution of 60,000 at 200 m/z) at a target of 3×10^6 ions. The 12 most intense ions were isolated and fragmented with HCD (target of 1×10^5 ions, maximum injection time of 28 ms, isolation window of 1.4 m/z, and collision energy of 28%) and detected in the Orbitrap (resolution of 15,000 at 200 m/z). Dynamic exclusion was set to 30 s.

For data analysis, raw MS files were processed within the MaxQuant environment (versions 1.5.3.15 and 1.6.0.15) using the MaxLFQ algorithm for label-free quantification and the integrated Andromeda search engine with a false discovery rate (FDR) of <0.01 at the protein and peptide levels (*32*, *53*, *54*). The search included variable modifications for oxidized methionine (M), acetylation (protein N-term), and phosphorylation (STY) and fixed modifications for carbamidomethyl (C). Up to two missed cleavages were allowed for protease digestion. Peptides with at least seven amino acids were considered for identification, and "match between runs" was enabled with a matching time window of 0.7 min to allow the quantification of MS1 features not identified in every measurement. Peptides and proteins were identified using a UniProt FASTA database from *Homo sapiens* (2015) containing 21,051 entries.

For bioinformatics analysis, the freely available software PERSEUS (*55*) (versions 1.5.4.1 and 1.6.1.3) and GraphPad Prism version 7.03 were used to perform all statistical and bioinformatics analyses and for visualization. To determine interaction partners, the proteins identified only by site modification or found in the decoy reverse database and the contaminants were filtered out before data analysis. MaxLFQ intensities were taken for quantification and transformed into $\log_2$ scale. Three biological replicates of each pulldown were grouped, and a minimum of three valid values was required in at least one group. Missing values were imputed on the basis of a normal distribution (width = 0.3, down-shift = 1.8). Significance was assessed by two-sample Student's t test (two-sided) including a permutation-based FDR of 5% and an S0 value of 0.1. For CARD11 phosphorylation analysis, the phosphopeptides found in the decoy reverse database and the contaminants were filtered out before data analysis. The intensities were taken for quantification and transformed into $\log_2$ scale. Three biological replicates of each pulldown were grouped, and a minimum of three valid values was required in at least one group. Missing values were imputed on the basis of a normal distribution (width = 0.3, down-shift = 1.8). We took the median of the phosphopeptide intensities in three biological replicates of each

MS no: RAabk3083/ED/POSTTRANSLATIONAL MODIFICATION, SIGNAL TRANSDUCTION

pulldown and normalized all values to the median intensity of the WT unstimulated conditions.

PKC in vitro kinase assay

N-terminally glutathione *S*-transferase (GST)–tagged CARD11 peptide (amino acids 885 to 901 of human CARD11 WT or S893A) was expressed in *Escherichia coli* BL21-CodonPlus (DE3)-RIPL cells and purified using GSTrap High Performance columns (GE Healthcare) as previously described in (*28*). For in vitro kinase assays, 100 ng of recombinant PKCθ (Thermo Fisher Scientific) was incubated with 1 μg of GST-CARD11 WT or S893A in 20 μl of kinase assay buffer [25 mM Mops (pH 7.2), 12.5 mM glycerol 2-phosphate, 25 mM $MgCl_2$, 5 mM EGTA, and 2 mM EDTA]. Freshly prepared DTT (0.25 mM) and adenosine 5′-triphosphate (ATP) (0.25 mM) were added to the samples, which were incubated for 1 hour at 30°C. SDS loading buffer (Roti-Load1, Roth) was added to stop the reaction, and samples were boiled for 5 min. Phosphorylation was assessed by Western blotting using phosphorylated Ser^{893} CARD11 antibody, and loading was checked by Coomassie staining.

Size exclusion chromatography

SEC was performed using ÄKTApurifier System in combination with a Superose 6 10/300 GL column according to the protocol of the manufacturer (GE Healthcare). For each run, extracts prepared from 1×10^8 Jurkat T cells were loaded and preparation of extracts was performed as described previously (*56*). Fractions (0.5 ml) were collected and analyzed by Western blot. MALT1 detection in SEC was performed with monoclonal rat anti-MALT1 (17C11) antibody.

Statistical analysis

All experiments showing quantifications were performed with three to seven biological replicates, and values represent means ± SEM. For quantification of proteomic data (Fig. 1C and fig. S1G), phosphopeptide intensity values were normalized according to the median of three control replicates (CK1α WT), and $\log_2$-transformed values were subjected to an unpaired *t* test to determine statistical significance of changes in CK1α WT P/I or CK1α KI P/I. For data shown in Figs. 3C and 5 (A and J) and figs. S3 (B and D) and S7C, values were normalized to CARD11 WT, and statistical significance was determined on the $\log_2$ fold changes to the normalized values by one-sample *t* test. To compare statistical significance between two groups (Figs. 1, D and E, and 2, B and C, and fig. S2, C to G), values were analyzed by unpaired Student's *t* test. To compare statistical significance between more than two groups, one-way analysis of variance (ANOVA) combined with Tukey's (Figs. 3, G and H, and 5C and figs. S4C and S7K) or Dunnett's (Fig. 4B) multiple comparisons tests was used. Statistical significance is indicated by *P* values or by asterisk: $*P < 0.05$, $**P < 0.01$, $***P < 0.001$, and $****P < 0.0001$. ns indicates not significant.

SUPPLEMENTARY MATERIALS

www.science.org/doi/10.1126/scisignal.abk3083
Figs. S1 to S8
Tables S1 and S2
Data files S1 and S2

View/request a protocol for this paper from *Bio-protocol*.

REFERENCES AND NOTES

1. I. Meininger, D. Krappmann, Lymphocyte signaling and activation by the CARMA1-BCL10-MALT1 signalosome. *Biol. Chem.* **397**, 1315–1333 (2016).
2. J. Ruland, L. Hartjes, CARD-BCL-10-MALT1 signalling in protective and pathological immunity. *Nat. Rev. Immunol.* **19**, 118–134 (2019).
3. M. Jaworski, M. Thome, The paracaspase MALT1: Biological function and potential for therapeutic inhibition. *Cell. Mol. Life Sci.* **73**, 459–473 (2016).
4. M. Di Pilato, E. Y. Kim, B. L. Cadilha, J. N. Prussmann, M. N. Nasrallah, D. Seruggia, S. M. Usmani, S. Misale, V. Zappulli, E. Carrizosa, V. Mani, M. Ligorio, R. D. Warner, B. D. Medoff, F. Marangoni, A. C. Villani, T. R. Mempel, Targeting the CBM complex causes Treg cells to prime tumours for immune checkpoint therapy. *Nature* **570**, 112–116 (2019).
5. A. Gewies, O. Gorka, H. Bergmann, K. Pechloff, F. Petermann, K. M. Jeltsch, M. Rudelius, M. Kriegsmann, W. Weichert, M. Horsch, J. Beckers, W. Wurst, M. Heikenwalder, T. Korn, V. Heissmeyer, J. Ruland, Uncoupling Malt1 threshold function from paracaspase activity results in destructive autoimmune inflammation. *Cell Rep.* **9**, 1292–1305 (2014).
6. M. Jaworski, B. J. Marsland, J. Gehrig, W. Held, S. Favre, S. A. Luther, M. Perroud, D. Golshayan, O. Gaide, M. Thome, Malt1 protease inactivation efficiently dampens immune responses but causes spontaneous autoimmunity. *EMBO J.* **33**, 2765–2781 (2014).
7. M. Rosenbaum, A. Gewies, K. Pechloff, C. Heuser, T. Engleitner, T. Gehring, L. Hartjes, S. Krebs, D. Krappmann, M. Kriegsmann, W. Weichert, R. Rad, C. Kurts, J. Ruland, Bcl10-controlled Malt1 paracaspase activity is key for the immune suppressive function of regulatory T cells. *Nat. Commun.* **10**, 2352 (2019).
8. D. Nagel, M. Vincendeau, A. C. Eitelhuber, D. Krappmann, Mechanisms and consequences of constitutive NF-κB activation in B-cell lymphoid malignancies. *Oncogene* **33**, 5655–5665 (2014).
9. H. Y. Lu, B. M. Bauman, S. Arjunaraja, B. Dorjbal, J. D. Milner, A. L. Snow, S. E. Turvey, The CBM-opathies-a rapidly expanding spectrum of human inborn errors of immunity caused by mutations in the CARD11-BCL10-MALT1 complex. *Front. Immunol.* **9**, 2078 (2018).
10. L. David, Y. Li, J. Ma, E. Garner, X. Zhang, H. Wu, Assembly mechanism of the CARMA1-BCL10-MALT1-TRAF6 signalosome. *Proc. Natl. Acad. Sci. U.S.A.* **115**, 1499–1504 (2018).
11. Q. Qiao, C. Yang, C. Zheng, L. Fontan, L. David, X. Yu, C. Bracken, M. Rosen, A. Melnick, E. H. Egelman, H. Wu, Structural architecture of the CARMA1/Bcl10/MALT1 signalosome: Nucleation-induced filamentous assembly. *Mol. Cell* **51**, 766–779 (2013).
12. F. Schlauderer, T. Seeholzer, A. Desfosses, T. Gehring, M. Strauss, K.-P. Hopfner, I. Gutsche, D. Krappmann, K. Lammens, Molecular architecture and regulation of BCL10-MALT1 filaments. *Nat. Commun.* **9**, 4041 (2018).
13. T. Seeholzer, S. Kurz, F. Schlauderer, S. Woods, T. Gehring, S. Widmann, K. Lammens, D. Krappmann, BCL10-CARD11 fusion mimics an active CARD11 seed that triggers constitutive BCL10 oligomerization and lymphocyte activation. *Front. Immunol.* **9**, 2695 (2018).
14. J. R. Bedsaul, N. M. Carter, K. E. Deibel, S. M. Hutcherson, T. A. Jones, Z. Wang, C. Yang, Y. K. Yang, J. L. Pomerantz, Mechanisms of regulated and dysregulated CARD11 signaling in adaptive immunity and disease. *Front. Immunol.* **9**, 2105 (2018).
15. R. P. Jattani, J. M. Tritapoe, J. L. Pomerantz, Cooperative control of caspase recruitment domain-containing protein 11 (CARD11) signaling by an unusual array of redundant repressive elements. *J. Biol. Chem.* **291**, 8324–8336 (2016).
16. R. P. Jattani, J. M. Tritapoe, J. L. Pomerantz, Intramolecular interactions and regulation of cofactor binding by the four repressive elements in the caspase recruitment domain-containing protein 11 (CARD11) inhibitory domain. *J. Biol. Chem.* **291**, 8338–8348 (2016).
17. Z. Wang, S. M. Hutcherson, C. Yang, R. P. Jattani, J. M. Tritapoe, Y. K. Yang, J. L. Pomerantz, Coordinated regulation of scaffold opening and enzymatic activity during CARD11 signaling. *J. Biol. Chem.* **294**, 14648–14660 (2019).
18. M. Lork, J. Staal, R. Beyaert, Ubiquitination and phosphorylation of the CARD11-BCL10-MALT1 signalosome in T cells. *Cell. Immunol.* **340**, 103877 (2019).
19. R. Matsumoto, D. Wang, M. Blonska, H. Li, M. Kobayashi, B. Pappu, Y. Chen, D. Wang, X. Lin, Phosphorylation of CARMA1 plays a critical role in T Cell receptor-mediated NF-kappaB activation. *Immunity* **23**, 575–585 (2005).
20. M. E. Moreno-Garcia, K. Sommer, C. Haftmann, C. Sontheimer, S. F. Andrews, D. J. Rawlings, Serine 649 phosphorylation within the protein kinase C-regulated domain down-regulates CARMA1 activity in lymphocytes. *J. Immunol.* **183**, 7362–7370 (2009).
21. K. Sommer, B. Guo, J. L. Pomerantz, A. D. Bandaranayake, M. E. Moreno-Garcia, Y. L. Ovechkina, D. J. Rawlings, Phosphorylation of the CARMA1 linker controls NF-kappaB activation. *Immunity* **23**, 561–574 (2005).
22. H. Shinohara, M. Behar, K. Inoue, M. Hiroshima, T. Yasuda, T. Nagashima, S. Kimura, H. Sanjo, S. Maeda, N. Yumoto, S. Ki, S. Akira, Y. Sako, A. Hoffmann, T. Kurosaki, M. Okada-Hatakeyama, Positive feedback within a kinase signaling complex functions as a switch mechanism for NF-kappaB activation. *Science* **344**, 760–764 (2014).
23. H. Shinohara, S. Maeda, H. Watarai, T. Kurosaki, IkappaB kinase beta-induced phosphorylation of CARMA1 contributes to CARMA1 Bcl10 MALT1 complex formation in B cells. *J. Exp. Med.* **204**, 3285–3293 (2007).

24. E. Wegener, A. Oeckinghaus, N. Papadopoulou, L. Lavitas, M. Schmidt-Supprian, U. Ferch, T. W. Mak, J. Ruland, V. Heissmeyer, D. Krappmann, Essential role for IkappaB kinase beta in remodeling Carma1-Bcl10-Malt1 complexes upon T cell activation. *Mol. Cell* **23**, 13–23 (2006).
25. D. Brenner, M. Brechmann, S. Rohling, M. Tapernoux, T. Mock, D. Winter, W. D. Lehmann, F. Kiefer, M. Thome, P. H. Krammer, R. Arnold, Phosphorylation of CARMA1 by HPK1 is critical for NF-kappaB activation in T cells. *Proc. Natl. Acad. Sci. U.S.A.* **106**, 14508–14513 (2009).
26. K. Ishiguro, T. Green, J. Rapley, H. Wachtel, C. Giallourakis, A. Landry, Z. Cao, N. Lu, A. Takafumi, H. Goto, M. J. Daly, R. J. Xavier, Ca^{2+}/calmodulin-dependent protein kinase II is a modulator of CARMA1-mediated NF-kappaB activation. *Mol. Cell. Biol.* **26**, 5497–5508 (2006).
27. N. Bidere, V. N. Ngo, J. Lee, C. Collins, L. Zheng, F. Wan, R. E. Davis, G. Lenz, D. E. Anderson, D. Arnoult, A. Vazquez, K. Sakai, J. Zhang, Z. Meng, T. D. Veenstra, L. M. Staudt, M. J. Lenardo, Casein kinase 1alpha governs antigen-receptor-induced NF-kappaB activation and human lymphoma cell survival. *Nature* **458**, 92–96 (2009).
28. T. Gehring, T. Erdmann, M. Rahm, C. Graß, A. Flatley, T. J. O'Neill, S. Woods, I. Meininger, O. Karayel, K. Kutzner, M. Grau, H. Shinohara, K. Lammens, R. Feederle, S. M. Hauck, G. Lenz, D. Krappmann, MALT1 phosphorylation controls activation of T lymphocytes and survival of ABC-DLBCL tumor cells. *Cell Rep.* **29**, 873–888.e810 (2019).
29. J. L. Pomerantz, Reconsidering phosphorylation in the control of inducible CARD11 scaffold activity during antigen receptor signaling. *Adv. Biol. Regul.* **79**, 100775 (2021).
30. V. Mayya, D. H. Lundgren, S. I. Hwang, K. Rezaul, L. Wu, J. K. Eng, V. Rodionov, D. K. Han, Quantitative phosphoproteomic analysis of T cell receptor signaling reveals system-wide modulation of protein-protein interactions. *Sci. Signal.* **2**, ra46 (2009).
31. S. Satpathy, S. A. Wagner, P. Beli, R. Gupta, T. A. Kristiansen, D. Malinova, C. Francavilla, P. Tolar, G. A. Bishop, B. S. Hostager, C. Choudhary, Systems-wide analysis of BCR signalosomes and downstream phosphorylation and ubiquitylation. *Mol. Syst. Biol.* **11**, 810 (2015).
32. J. Cox, M. Mann, MaxQuant enables high peptide identification rates, individualized p.p.b.-range mass accuracies and proteome-wide protein quantification. *Nat. Biotechnol.* **26**, 1367–1372 (2008).
33. G. Lenz, R. E. Davis, V. N. Ngo, L. Lam, T. C. George, G. W. Wright, S. S. Dave, H. Zhao, W. Xu, A. Rosenwald, G. Ott, H. K. Muller-Hermelink, R. D. Gascoyne, J. M. Connors, L. M. Rimsza, E. Campo, E. S. Jaffe, J. Delabie, E. B. Smeland, R. I. Fisher, W. C. Chan, L. M. Staudt, Oncogenic CARD11 mutations in human diffuse large B cell lymphoma. *Science* **319**, 1676–1679 (2008).
34. C. A. Ma, J. R. Stinson, Y. Zhang, J. K. Abbott, M. A. Weinreich, P. J. Hauk, P. R. Reynolds, J. J. Lyons, C. G. Nelson, E. Ruffo, B. Dorjbal, S. Glauzy, N. Yamakawa, S. Arjunaraja, K. Voss, J. Stoddard, J. Niemela, Y. Zhang, S. D. Rosenzweig, J. J. McElwee, T. DiMaggio, H. F. Matthews, N. Jones, K. D. Stone, A. Palma, M. Oleastro, E. Prieto, A. R. Bernasconi, G. Dubra, S. Danielian, J. Zaiat, M. A. Marti, B. Kim, M. A. Cooper, N. Romberg, E. Meffre, E. W. Gelfand, A. L. Snow, J. D. Milner, Germline hypomorphic CARD11 mutations in severe atopic disease. *Nat. Genet.* **49**, 1192–1201 (2017).
35. A. L. Snow, W. Xiao, J. R. Stinson, W. Lu, B. Chaigne-Delalande, L. Zheng, S. Pittaluga, H. F. Matthews, R. Schmitz, S. Jhavar, S. Kuchen, L. Kardava, W. Wang, I. T. Lamborn, H. Jing, M. Raffeld, S. Moir, T. A. Fleisher, L. M. Staudt, H. C. Su, M. J. Lenardo, Congenital B cell lymphocytosis explained by novel germline CARD11 mutations. *J. Exp. Med.* **209**, 2247–2261 (2012).
36. R. E. Davis, V. N. Ngo, G. Lenz, P. Tolar, R. M. Young, P. B. Romesser, H. Kohlhammer, L. Lamy, H. Zhao, Y. Yang, W. Xu, A. L. Shaffer, G. Wright, W. Xiao, J. Powell, J. K. Jiang, C. J. Thomas, A. Rosenwald, G. Ott, H. K. Muller-Hermelink, R. D. Gascoyne, J. M. Connors, N. A. Johnson, L. M. Rimsza, E. Campo, E. S. Jaffe, W. H. Wilson, J. Delabie, E. B. Smeland, R. I. Fisher, R. M. Braziel, R. R. Tubbs, J. R. Cook, D. D. Weisenburger, W. C. Chan, S. K. Pierce, L. M. Staudt, Chronic active B-cell-receptor signalling in diffuse large B-cell lymphoma. *Nature* **463**, 88–92 (2010).
37. D. Nagel, S. Spranger, M. Vincendeau, M. Grau, S. Raffegerst, B. Kloo, D. Hlahla, M. Neuenschwander, J. Peter von Kries, K. Hadian, B. Dorken, P. Lenz, G. Lenz, D. J. Schendel, D. Krappmann, Pharmacologic inhibition of MALT1 protease by phenothiazines as a therapeutic approach for the treatment of aggressive ABC-DLBCL. *Cancer Cell* **22**, 825–837 (2012).
38. W. H. Wilson, R. M. Young, R. Schmitz, Y. Yang, S. Pittaluga, G. Wright, C. J. Lih, P. M. Williams, A. L. Shaffer, J. Gerecitano, S. de Vos, A. Goy, V. P. Kenkre, P. M. Barr, K. A. Blum, A. Shustov, R. Advani, N. H. Fowler, J. M. Vose, R. L. Elstrom, T. M. Habermann, J. C. Barrientos, J. McGreivy, M. Fardis, B. Y. Chang, F. Clow, B. Munneke, D. Moussa, D. M. Beaupre, L. M. Staudt, Targeting B cell receptor signaling with ibrutinib in diffuse large B cell lymphoma. *Nat. Med.* **21**, 922–926 (2015).
39. M. Bardet, A. Unterreiner, C. Malinverni, F. Lafossas, C. Vedrine, D. Boesch, Y. Kolb, D. Kaiser, A. Gluck, M. A. Schneider, A. Katopodis, M. Renatus, O. Simic, A. Schlapbach, J. Quancard, C. H. Regnier, G. Bold, C. Pissot-Soldermann, J. M. Carballido, J. Kovarik, T. Calzascia, F. Bornancin, The T-cell fingerprint of MALT1 paracaspase revealed by selective inhibition. *Immunol. Cell Biol.* **96**, 81–99 (2018).
40. J. P. Evenou, J. Wagner, G. Zenke, V. Brinkmann, K. Wagner, J. Kovarik, K. A. Welzenbach, G. Weitz-Schmidt, C. Guntermann, H. Towbin, S. Cottens, S. Kaminski, T. Letschka, C. Lutz-Nicoladoni, T. Gruber, N. Hermann-Kleiter, N. Thuille, G. Baier, The potent protein kinase C-selective inhibitor AEB071 (sotrastaurin) represents a new class of immunosuppressive agents affecting early T-cell activation. *J. Pharmacol. Exp. Ther.* **330**, 792–801 (2009).
41. A. Oeckinghaus, E. Wegener, V. Welteke, U. Ferch, S. C. Arslan, J. Ruland, C. Scheidereit, D. Krappmann, Malt1 ubiquitination triggers NF-kappaB signaling upon T-cell activation. *EMBO J.* **26**, 4634–4645 (2007).
42. S. Li, X. Yang, J. Shao, Y. Shen, Structural insights into the assembly of CARMA1 and BCL10. *PLOS ONE* **7**, e42775 (2012).
43. H. Hara, T. Yokosuka, H. Hirakawa, C. Ishihara, S. Yasukawa, M. Yamazaki, H. Koseki, H. Yoshida, T. Saito, Clustering of CARMA1 through SH3-GUK domain interactions is required for its activation of NF-κB signalling. *Nat. Commun.* **6**, 5555 (2015).
44. R. R. McCully, J. L. Pomerantz, The protein kinase C-responsive inhibitory domain of CARD11 functions in NF-kappaB activation to regulate the association of multiple signaling cofactors that differentially depend on Bcl10 and MALT1 for association. *Mol. Cell. Biol.* **28**, 5668–5686 (2008).
45. M. E. Moreno-Garcia, K. Sommer, H. Shinohara, A. D. Bandaranayake, T. Kurosaki, D. J. Rawlings, MAGUK-controlled ubiquitination of CARMA1 modulates lymphocyte NF-kappaB activity. *Mol. Cell. Biol.* **30**, 922–934 (2010).
46. G. Schimmack, A. C. Eitelhuber, M. Vincendeau, K. Demski, H. Shinohara, T. Kurosaki, D. Krappmann, AIP augments CARMA1-BCL10-MALT1 complex formation to facilitate NF-κB signaling upon T cell activation. *Cell Commun. Signal.* **12**, 49 (2014).
47. H. Y. Lu, C. M. Biggs, G. Blanchard-Rohner, S. Y. Fung, M. Sharma, S. E. Turvey, Germline CBM-opathies: From immunodeficiency to atopy. *J. Allergy Clin. Immunol.* **143**, 1661–1673 (2019).
48. D. R. Myers, J. Zikherman, J. P. Roose, Tonic signals: Why do lymphocytes bother? *Trends Immunol.* **38**, 844–857 (2017).
49. A. J. Ninfa, A. E. Mayo, Hysteresis vs. graded responses: The connections make all the difference. *Sci. STKE* **2004**, pe20 (2004).
50. I. Meininger, R. A. Griesbach, D. Hu, T. Gehring, T. Seeholzer, A. Bertossi, J. Kranich, A. Oeckinghaus, A. C. Eitelhuber, U. Greczmiel, A. Gewies, M. Schmidt-Supprian, J. Ruland, T. Brocker, V. Heissmeyer, F. Heyd, D. Krappmann, Alternative splicing of MALT1 controls signalling and activation of CD4(+) T cells. *Nat. Commun.* **7**, 11292 (2016).
51. J. Rappsilber, Y. Ishihama, M. Mann, Stop and go extraction tips for matrix-assisted laser desorption/ionization, nanoelectrospray, and lc/ms sample pretreatment in proteomics. *Anal. Chem.* **75**, 663–670 (2003).
52. N. A. Kulak, G. Pichler, I. Paron, N. Nagaraj, M. Mann, Minimal, encapsulated proteomic-sample processing applied to copy-number estimation in eukaryotic cells. *Nat. Methods* **11**, 319–324 (2014).
53. J. Cox, M. Y. Hein, C. A. Luber, I. Paron, N. Nagaraj, M. Mann, Accurate proteome-wide label-free quantification by delayed normalization and maximal peptide ratio extraction, termed MaxLFQ. *Mol. Cell. Proteomics* **13**, 2513–2526 (2014).
54. J. Cox, N. Neuhauser, A. Michalski, R. A. Scheltema, J. V. Olsen, M. Mann, Andromeda: A peptide search engine integrated into the MaxQuant environment. *J. Proteome Res.* **10**, 1794–1805 (2011).
55. S. Tyanova, T. Temu, P. Sinitcyn, A. Carlson, M. Y. Hein, T. Geiger, M. Mann, J. Cox, The Perseus computational platform for comprehensive analysis of (prote)omics data. *Nat. Methods* **13**, 731–740 (2016).
56. A. Stangl, P. R. Elliott, A. Pinto-Fernandez, S. Bonham, L. Harrison, A. Schaub, K. Kutzner, K. Keusekotten, P. T. Pfluger, F. El Oualid, B. M. Kessler, D. Komander, D. Krappmann, Regulation of the endosomal SNX27-retromer by OTULIN. *Nat. Commun.* **10**, 4320 (2019).
57. Y. Perez-Riverol, A. Csordas, J. Bai, M. Bernal-Llinares, S. Hewapathirana, D. J. Kundu, A. Inuganti, J. Griss, G. Mayer, M. Eisenacher, E. Pérez, J. Uszkoreit, J. Pfeuffer, T. Sachsenberg, S. Yilmaz, S. Tiwary, J. Cox, E. Audain, M. Walzer, A. F. Jarnuczak, T. Ternent, A. Brazma, J. A. Vizcaíno, The PRIDE database and related tools and resources in 2019: Improving support for quantification data. *Nucleic Acids Res.* **47**, D442–D450 (2019).

Acknowledgments: We thank K. Demski and I. Paron for excellent technical assistance. We thank A. Gewies for scientific input. We thank T. Straub and A. Yeroslaviz for advice on statistical testing. **Funding:** This work was supported by Deutsche Krebshilfe award grant 70112622 and the Deutsche Forschungsgemeinschaft (DFG) (Project ID 360372040 – SFB 1335 P07 to D.K.) **Author contributions:** K.K. designed, performed, and analyzed most of the experiments. S.W. conceived and helped to perform experiments, analyzed and interpreted data, and helped to write the manuscript. O.K. and M.M. conceived, performed, and analyzed MS experiments with material provided by K.K., and T.G., H.Y., C.G., N.W., M.J.T., and T.S.

MS no: RAabk3083/ED/POSTTRANSLATIONAL MODIFICATION, SIGNAL TRANSDUCTION

performed or contributed to specific experiments. A.F. and R.F. generated, subcloned, and provided the CARD11 phosphorylated Ser^{893} antibody. D.K. conceived the project, designed the experiments, analyzed data, and wrote the paper. All authors have read and approved the manuscript. **Competing interests:** D.K. is a scientific advisor of Monopteros Therapeutics Inc., Boston. The other authors declare that they have no competing interests. **Data and materials availability:** MS raw data on CARD11 protein interactions and phosphorylation have been deposited to the ProteomeXchange Consortium through the PRIDE (*57*) partner repository with the dataset identifier PXD025198. All other data needed to evaluate the conclusions in the paper are present in the paper or the Supplementary Materials.

Submitted 5 July 2021
Accepted 31 January 2022
Published 1 March 2022
10.1126/scisignal.abk3083

Abstract

One-sentence summary: PKCθ-mediated phosphorylation of the CBM component CARD11 restrains antigen receptor–induced activation of T and B cells.

Editor's Summary:
Putting the brakes on lymphocyte activation

Stimulation of antigen receptors on T or B cells leads to the formation of a complex consisting of the scaffolding protein CARD11, the linking factor BCL10, and the protease MALT1 (CBM), which ultimately results in T or B cell activation. The ability of CARD11 to recruit BCL10 and MALT1 is regulated by multiple phosphorylation events mediated by various kinases. Using biochemical techniques and T and B cell lines expressing phosphorylation mutants of CARD11, Kutzner *et al.* identified Ser^{893} as an inhibitory phosphorylation site that restrained antigen receptor–induced CBM formation and lymphocyte activation. This phosphorylation event prevented the activation of T cells without coreceptor stimulation and sensitized B cell lymphomas to inhibitors used to treat this cancer type. Because PKCθ also mediates stimulatory phosphorylation events for CARD11, the authors speculate that the combination of stimulatory and inhibitory phosphorylation events sets signaling thresholds for lymphocyte activation.

MS no: RAabk3083/ED/POSTTRANSLATIONAL MODIFICATION, SIGNAL TRANSDUCTION